Published in final edited form as:

Adv Mater. 2017 June ; 29(23): . doi:10.1002/adma.201605096.

From Flatland to Spaceland: Higher Dimensional Patterning with Two-Dimensional Materials

Dr. Po-Yen Chen,
School of Engineering, Institute for Molecular and Nanoscale Innovation, Brown University, Providence, RI 02912

Muchun Liu,
School of Engineering, Institute for Molecular and Nanoscale Innovation, Brown University, Providence, RI 02912

Department of Chemistry, Institute for Molecular and Nanoscale Innovation Brown University, Providence, RI 02912

Dr. Zhongying Wang,
School of Engineering, Institute for Molecular and Nanoscale Innovation, Brown University, Providence, RI 02912

Prof. Robert H. Hurt, and
School of Engineering, Institute for Molecular and Nanoscale Innovation, Brown University, Providence, RI 02912

Prof. Ian Y. Wong
School of Engineering, Institute for Molecular and Nanoscale Innovation Brown University, Providence, RI 02912

Abstract

The creation of three-dimensional (3D) structures from two-dimensional (2D) nanomaterial building blocks enables novel chemical, mechanical or physical functionalities that cannot be realized with planar thin films or in bulk materials. In this Progress Report, we review the use of emerging 2D materials to create complex out-of-plane surface topographies and 3D material architectures. We focus on recent approaches that yield periodic textures or patterns, and present four techniques as case studies: (i) wrinkling and crumpling of planar sheets, (ii) encapsulation by crumpled nanosheet shells, (iii) origami folding and kirigami cutting to create programmed curvature, and (iv) 3D printing of 2D material suspensions. Work to date in this field has primarily used graphene and graphene oxide as the 2D building blocks, and we consider how these unconventional approaches may be extended to alternative 2D materials and their heterostructures. Taken together, these emerging patterning and texturing techniques represent an intriguing alternative to conventional materials synthesis and processing methods, and are expected to contribute to the development of new composites, stretchable electronics, energy storage devices, chemical barriers, and biomaterials.

Correspondence to: Po-Yen Chen; Robert H. Hurt; Ian Y. Wong.

Keywords

2D materials; self-assembly; mechanical deformation; hierarchical structure; origami and kirigami; 3D printing

1. Introduction

Atomically thin two-dimensional (2D) materials such as graphene can display extraordinary chemical, physical and mechanical properties, but exploiting these properties for technological applications often requires nanosheet assembly into higher dimensional architectures.[1,2] Historically, precision measurements of 2D material chemical and physical properties have utilized samples prepared by exfoliation techniques or controlled growth from the vapor phase.[3] The deposition of patterned 2D materials has analogies with thin film processing in semiconductor fabrication and holds great promise for the direct integration of 2D materials into integrated circuits.[4] Although top-down patterning techniques are effective for well-controlled planar patterns at the wafer scale, they may be less useful for patterning very large areas, creating out-of-plane surface topographies, curved geometries, or soft materials.[5]

In many cases, 2D materials are produced as dispersed nanosheets of sub-micron to micron-scale lateral dimension in aqueous solutions or organic solvents, particularly when prepared using solution-based growth or exfoliation techniques.[6–8] When suspended in a fluid phase, nanosheets exhibit complex behaviors that include self-avoidance and uniform dispersion due to electrostatic repulsion, aggregation (to disordered flocs) or (re)stacking to aligned 2D multilayer flocs, liquid crystal alignment driven by large excluded volume effects associated with very high aspect ratio and high concentration, interfacial accumulation, and mechanical deformation by weak electrostatic or van der Waals forces in the liquid phase or at the liquid-air interface or deposition substrates.[9] Based on the importance of weak forces, nanosheet assemblies can be regarded as soft materials,[10] and there is a significant literature on their fundamental behavior as colloids,[10–12] surfactants,[10,13,14] and liquid crystals.[10,12,15–17] While nanosheet assemblies have mechanical properties typical of soft materials, they retain other characteristic physicochemical properties and functions of the hard-material 3D parent inorganic crystals from which they originate, such as electronic bandgaps, thermal and chemical stability.

Historically, studies of the self-organization of 2D materials into bulk 3D architectures has been carried out using graphene or graphene oxide (GO) and can be broadly classified into three approaches: (i) stacking to create multilayer films with a significant third dimension, (ii) association in liquid phases to form 3D gels or foams, or (iii) deposition onto pre-existing 3D sacrificial templates. Stacking assembly is widely used to make coatings or free-standing papers used in applications as barriers, separation membranes, or electrodes.[18–21] Stacking processes may also involve molecular or nanoparticle additives or functional groups that interrupt alignment to produce engineered porosity or adjust the width of interlayer gallery spaces in GO films, which have been proposed as molecular sieve membranes.[22–24] Gelation has been used to convert nanosheet suspensions into

macroporous 3D hydrogels or organogels, which can be converted to xerogels by simple drying or low-density aerogels by freeze drying or supercritical drying.[25–28] Gelation can also be induced by colloidal destablization through salt addition,[12] through chemical reduction of GO, which removes functional groups that carry the negative charge involved in electrostatic repulsion[25,29] or through covalent or non-covalent cross linking[26,27]. Finally, many ordered 3D graphene structures have been fabricated by CVD, electrophoretic deposition (EPD),[30–32] or nanosheet deposition from solution onto/into prefabricated 3D templates, including metal foams,[33] 3D printed metal grids,[34] emulsion droplets,[35] and materials with regular porosity such as zeolites,[36] which are subsequently removed by dissolution or evaporation. These three assembly modes for creating bulk higher-dimensional architectures have received significant attention in the primary and review literature,[37] and thus will not be the main focus here.

In this Progress Report, we focus on several emerging approaches to the fabrication of 3D architectures,* emphasizing the creation of microstructural or textural patterns with defined length scales by directed assembly and patterning of nanosheet building blocks: (1) wrinkling and crumpling of 2D material films on flat substrates using mismatched mechanical deformation; (2) wrapping and crumpling of 2D materials around curved objects; (3) folding (origami) and cutting (kirigami) using 2D materials; and (4) 3D printing from 2D nanosheet suspensions (Figure 1). These four techniques for processing and fabrication may facilitate the application of 2D materials in energy storage,[38] environmental mediation,[39] catalysis,[40] controlled wetting surfaces,[41] bioelectronic interfaces and biomaterial implants.[42] To date, these patterning techniques have primarily been implemented using graphene and GO, but they could be utilized with a wide variety of 2D materials. Thus, we conclude with the potential to extend this field to 2D materials "beyond graphene" and offer our perspectives on future directions.

2. Wrinkling and Crumpling of 2D Material Films on Flat Substrates

2D materials often display complex surface topographies since they are much easier to bend out-of-plane than stretch in-plane.[43] These morphological surface instabilities can be thermally-induced equilibrium ripple features exhibited by extended monolayers[44] or can be programmed by manipulating interfacial conditions, often through some external stimulus.[45] For instance, continuous graphene monolayers have been grown by chemical vapor deposition on copper and transferred onto a pre-stretched elastomeric substrate.[46,47] The subsequent relaxation of the elastomeric substrate and the mechanical mismatch with the stiff graphene resulted in the formation of out-of-plane surface patterns (Figure 2a). In particular, the relaxation of initially smooth films (Figure 2b) resulted in regular periodic wrinkles for uniaxial compression (Figure 2c) and disordered crumples for biaxial compression (Figure 2d). It should be noted that the fabrication and transfer of monolayer graphene can be laborious and difficult to scale. As an alternative, we and others have

*Note there are many carbon materials whose structures can be conceptually modelled as collections of curved graphene layers, with or without 5- or 7-membered rings, yet are not fabricated by assembling isolated 2D nanosheet building blocks. Examples include carbon nanotubes, nanofibers, nanohorns, and carbon onions, and these materials are not covered here. Such materials typically form through atomic-level assembly, rather than nanosheet assembly, and have been the subject of extensive research and numerous prior reviews.

deposited GO nanosheets from solution onto elastomeric substrates,[48–50] which exhibits decreased mechanical stiffness relative to monolayer graphene.[44] Nevertheless, this approach yields qualitatively similar surface topographies as well as being facile and scalable using solution casting and spraying techniques.

These wrinkling and crumpling behaviors have been modeled using classical buckling theories initially developed for the failure of multilayered composite structures.[51–53] For small deformations and thick substrates, the characteristic wrinkling wavelength can be approximated as $\lambda = 2\pi h(E_c/3E_s)^{1/3}$, where h is the coating thickness, E_c and E_s are the plane strain elastic moduli for the coating and substrate, respectively.[54,55] Thus, the periodicity of the wrinkled architectures can be experimentally tuned by changing the coating thickness. In the limit of larger deformations, 2D material coatings can detach or delaminate from the substrate, driving higher amplitude features that deviate from this classical buckling treatment. Numerical modeling of these behaviors indicate that the onset of delamination occurs when the strain mismatch energy surpasses the adhesion energy between the coating and substrate.[56] Experimentally, we have observed that large pre-strains can result in sawtooth-like architectures with nearly straight slopes and sharp curvatures at the peaks (Figure 2e, arrow 1 and 2).[43] Moreover, some primary peaks are observed to collapse onto their neighbors to create high amplitude double ridges (Figure 2e, arrow 3). We also found that by fixing the sides of the pre-stretched films, the longitudinal cracks can be reduced by suppressing the transverse Poisson expansion during the wrinkling process. One metric of surface texturing is the degree of buckling (d_b), which compares the integrated surface area with the projected area.[45] Interestingly, this parameter depends on the substrate pre-strain and Poisson's ratio of the coating, but not on the film thickness. Altogether, the wavelengths and amplitudes of these self-organized surface patterns can be systematically tuned by the substrate thickness, stiffness and pre-strain.

Stress relaxation can also occur through thermal actuation of pre-stressed "shape memory" polymer substrates.[57] The thermally activated substrates consist of pre-stretched thermoplastics (*e.g.*, polystyrene, polyolefin), often known as "shrink film". In this approach, heating the samples above the glass transition temperature (~110°C) releases the pre-strain, causing the substrate to contract. For instance, a polymer-GO composite was deposited on a shrink film using sequential layer-by-layer deposition, which self-organized into crumpled architectures with varying complexity with increasing thermal treatment.[58] Alternatively, monolayer graphene was transferred to a shrink film substrate and formed uniform arrays of graphene wrinkles or crumples after contraction.[59] The wrinkling wavelength and crumpling size of surface patterns could be simply controlled by several processing parameters, including compressive strain and graphene thickness (Figure 2f). Additional complexity was achieved by selective heating of the substrate using infrared laser irradiation, which resulted in localized crumpling (Figure 2g,h).

We recently demonstrated more sophisticated hierarchical 2D material architectures by applying repeated deformation steps, thus surpassing previous wrinkling or crumpling approaches that result from only a single deformation step.[60] This fabrication approach was based on the ability to gently detach the GO coating from a contracted thermoplastic substrate and deposit them intact onto a new substrate. By iterating on this process, we

formed hierarchical architectures with a multi-generational “lineage” defined by the programmed sequence of biaxial or unidirectional contraction, where the 1D contraction step can be aligned parallel or perpendicular to the previous step (Figure 3). This sequential patterning approach enables the design of feature sizes and orientations across multiple length scales. Remarkably, the structural features and orientational order were retained across multiple mechanical deformations, resulting in sequence-dependent surface topographies with structural “memory” of the earlier deformation modes.

Higher-dimensional architectures are generally advantageous to enhance interfacial interactions and activity. In supercapacitors, the energy storage capacity scales with the effective surface area of the electrode, which can be enhanced by the use of surface textured nanomaterials.[61] As an example, our multigenerational graphene structures display distinct electrochemical behaviors with increasing surface texturing. The cyclic voltammetry curves of the CV curves of G_1 (one-time contraction), G_2 (two-time), and G_3 (three-time) graphene electrodes were measured and compared with the planar graphene electrode (G_0) in Figure 4a.[60] We found that G_3 electrodes achieved two-fold, five-fold, and twenty-fold larger current densities than G_2, G_1, and G_0 electrodes, respectively. This improvement mainly originated from the extreme compression of graphene sheets, which increased the areal density without compromising the electron collection resistance. Similarly, the charge/discharge rate for lithiumion batteries can be improved by increased contact area between the fluid electrolyte and solid electrode.[62] Finally, electrochemical biosensors can also display improved performance when increased surface area facilitates enhanced redox currents, as well as improving the accessibility of surface-immobilized receptors.[63] Nevertheless, it should be noted that increased surface areas may also result in unwanted electrochemical reactions, which may disrupt cycling and diminish device lifetime.

Convoluted graphene structures can be further patterned at the nanoscale by using block-copolymer lithography, followed by decoration using catalyst nanoparticles (*i.e.*, Pt). The crumpled structures largely increase the areal density of catalytic Pt particles and also provide high surface wettability that facilitates H_2 release from the electrode surface (inset of Figure 4b). The Pt-graphene crumpled electrodes therefore demonstrate superior catalytic performance of hydrogen evolution reaction (HER) over planar Pt-graphene electrodes (Figure 4b).[64] These customized crumpling/wrinkling processes have also provided technological advantages in various applications, including photodetectors[65] and sensors.[66]

Another exciting property of these highly convoluted 2D material coatings is their accordion-like flexibility. This property is particularly useful for stretchable electronics, which should remain intact and function without deterioration even under extreme deformations. For instance, 2D materials can be utilized as dielectric elastomer actuators (DEA) which transduce electric fields into large mechanical deformations.[67] These capacitor-like devices consist of a thin elastomeric (dielectric) spacer sandwiched between two compliant electrodes. The application of a potential difference across the electrodes results in an electrostatic force between them, which squeezes the dielectric layer. DEA reliability is limited by the compliance of the electrode material, which fractures under large deformations. Instead, wrinkled and partially delaminated graphene electrodes display large

and rapid actuation (100% area increase) relative to comparable flat electrodes (Figure 4c).[41,46] This deformability could be further enhanced by forming a mechanical composite of 2D material with a soft polymer. For instance, microcrumpled GO electrode structures were fabricated using thermo-mechanical shrinking were then infiltrated with a dilute silicone elastomer (PDMS).[68] These GO/PDMS composites demonstrated stable electrical conductivity and tolerated reversible deformation for up to 500 cycles without failure.

Finally, textured 2D materials are exciting as biomaterials due to their unique surface chemistry and nanoscale topographies. It has long been recognized that living cells can be influenced by submicron surface features through “contact guidance”.[69] Moreover, mammalian cells can adhere preferentially to 2D materials, which may arise due to enhanced adsorption of biomolecules to the unique surface chemistry.[70] We have recently investigated how human and mouse fibroblasts adhere to topographically patterned GO surfaces.[48] On flat GO substrates, both fibroblast types displayed random orientations (Figure 4d). Instead, on wrinkled GO substrates, fibroblasts aligned preferentially along the wrinkles and displayed a highly-elongated, bipolar morphology, likely due to mechanical confinement (Figure 4e). Overall, engineering 2D materials with multiscale topographic cues and defined surface chemistries represent a promising approach to manipulate cell-material interactions. More generally, these soft composite structures may be advantageous for applications involving mechanical deformation, particularly biotic-abiotic interfaces.[71] Nevertheless, additional characterization of 2D material adhesion to substrates will be necessary, particularly after prolonged mechanical cycling. Finally, our initial demonstration of transfer techniques may facilitate scale-up of textured 2D materials for deposition on unconventional materials, curved surfaces and large areas.

3. Wrapping and Crumpling of 2D Materials around Curved Objects

Microencapsulation in thin solid shells is often advantageous in the pharmaceutical and life sciences, food technology, cosmetics and cleaning.[72] In particular, 2D materials can be stacked into ultrathin, mechanically robust coatings with tunable molecular permeability.[24,73,74] An exciting variation of this approach is to prepare such planar coatings on 3D geometries to serve as encapsulation shells. In the limit of large cargos with diameter much larger than the nanosheet width, 2D material films are nearly continuous since the local curvature is relatively small and the constituent nanosheets are allowed to adopt essentially planar configurations. As a consequence, these spherical 2D material coatings display chemical barrier properties comparable to those measured for flat coatings.[75] Instead, for smaller spherical cargoes, the required positive Gaussian curvature drives nanosheet buckling[76] and crumpling to produce porous, permeable shells.[75] The radius of such a crumpled sphere, R, can be scaled to the unfolded length of a thin sheet L (on each side) and a fractal dimension D: $R \sim L^{2/D}$, where the lower limit $D \sim 2$ corresponds to a loose packing and the upper limit $D \sim 3$ corresponds to a denser packing.[77]

Experimentally, crumpled microparticles have been realized by aerosolization of dispersed GO nanosheets leading to isotropic compression and nanosheet buckling during droplet drying (Figure 5a).[78] An aqueous dispersion of micrometer sized GO nanosheets was nebulized into aerosol droplets, which were then passed through a preheated tube furnace

with nitrogen gas at 800 °C. The rapid evaporation of aerosol droplets leads to capillary compression on the GO nanosheets and achieves the final structure as a crumpled microparticle (Figure 5b). The GO sheets could be thermally treated into reduced GO (rGO) with a corresponding color change from brown to black. The crumpled rGO nanoparticles were reported to be resistant to aggregation in both solution and dried states, and remained dispersible.[78]

In the droplet microenvironment, the surface tension acts as a confinement force that drives compression and irreversible crumpling as the droplet radius decreases.[79,80] The confinement force increased with decreasing GO thickness and Young's modulus, which could be tuned to control microparticle size.[81] The confinement force also increased with faster evaporation rates, resulting in smaller microparticles.[82] When pristine graphene was used instead of GO, spray drying resulted in a multifaced, dimpled morphology, suggesting that the elasticity and surface chemistry were also important for this phenomenon.[83] The crumpling of pristine graphene nanosheets was reported to be reversed upon rehydration with an appropriate solvent (*e.g.*, water). Finally, hierarchical microparticles could be prepared by a two-stage process.[84] First, GO nanosheets were self-assembled into nanospheres by tuning their electrostatic interactions through the ionic strength of the solution. These GO nanospheres were then aerosolized, resulting in "super-assembled" GO clusters. These clusters displayed enhanced thermal stability, while retaining their mass after oxidation.

We have further investigated the self-assembly mechanism for encapsulation and adapted this approach for creation of core-shell structures by co-suspending nanoparticle "cargos" in the feed GO suspension.[85] These aerosol droplets shrank rapidly due to evaporation of the aqueous phase, resulting in the self-organization of nanoparticles and GO nanosheets through several stages (Figure 5c). First, the GO nanosheets were sparsely located towards the droplet periphery and dragged inward as the droplet volume is reduced. The rapid drying process caused a spontaneous segregation of particle types, leading to a core-shell structure with cargo in the interior and an rGO encapsulation shell at the periphery. After encapsulating the nanoparticles, these sheets further aggregated with extensive wrinkling before achieving the final structure as a crumpled and plastically deformed particle that bears strong resemblance to "collapsed sacks." This approach has also been used with precursor solutions of metal ions rather than pre-fabricated nanoparticles.[86] As the aqueous solution evaporated, the metal ions spontaneously nucleated nanocrystals on the internal and external surface of the crumpled rGO shells (Figure 5d).

These crumpled rGO shells immobilize nanoparticle cargos, but do not function as tight molecular barriers due to their porous structure, suggesting applications in catalysis as "nanoreactors" that host controlled chemical reactions in their internal cavities.[87] Encapsulation in graphene nanoreactors can, in some cases (*e.g.*, Cu, Ag), enhance the metal oxidation rate in aqueous media, which is attributed to the electron transfer from the metal core to conductive graphene, allowing the reduction of molecular oxygen on the high-area graphene shell.

One limitation of the aerosol-assisted crumpling technique is the scalability of the ultrasonic droplet generation step. An alternative approach utilized iron oxide particles as hard templates, which were encapsulated by GO and simultaneously chemically etched and reduced.[88] This treatment resulted in the shrinkage of the outer GO layers into the crumpled forms (Figure 5e). These crumpled graphene microparticles could be further assembled into macroporous 3D architectures by solvent casting or compression molding without the need for binding agents. Alternatively, diphenylalanine peptides were used to assemble GO nanosheets into peptide-GO core-shell nanowires, and subsequent high-temperature calcination removed the soft templates and generated hollow graphene nanotubes with high aspect ratios.[89] Another approach utilized a non-planar aprotic anti-solvent (hexane), which is incapable of dispersing GO nanosheets due to the lack of interaction with the oxygen surface groups.[90] Instead, the oxygen surface groups form hydrogen bonds between regions within the GO nanosheets, which results in crumpling rather than re-stacking of the nanosheets.

The π-π stacked ridges and strain-hardening properties make the crumpled graphene balls remarkably stable against aggregation not only in solution but also in solid state. The flowchart in Figure 6a shows the surface areas of planar GO stacking and crumpled GO microparticles after various treatments.[78] The initial planar GO stacking demonstrated a low specific surface area (<5 $m^2\ g^{-1}$), and their subsequent surface areas are extremely sensitive to their processing history (*e.g.*, thermal treatment, solution processing, high-pressure compression). In contrast, crumpled GO microparticles have a significantly higher initial surface area (82 $m^2\ g^{-1}$) due to their open structure. They always yielded higher surface area graphene products regardless of heating rate: (344 $m^3\ g^{-1}$ for slow heating and 567 $m^2\ g^{-1}$ for rapid heating). Compared to the graphene sheets, crumpled microparticles exhibited consistently higher and much more stable surface areas after undergoing comparable processing.

Crumpled GO microparticles are advantageous for certain technological applications due to their high surface area, flexibility, internal free volume, and geometry-based resistance to surface area loss by restacking. In particular, electrodes for battery and supercapacitor applications require high surface area, short electrolyte transport distances, as well as mechanical robustness under large volume changes.[91] For instance, the crumpled graphene microparticles demonstrate higher specific capacitance (150 F g^{-1}) than wrinkled (140 F g^{-1}) and flat graphene sheets (120 F g^{-1}) (Figure 6b).[92] Moreover, the uniformly distributed free space inside and between the crumpled particles can facilitate charge transport, especially at high current density and high mass loading, leading to stable specific capacitance and rate capability. By co-suspending the monolayer GO with a wide variety of nanoparticles (*e.g.*, Mn_3O_4, SnO_2,[86] Co_3O_4,[93] and Si[94,95]) core-shell nanostructures have demonstrated improved electrochemical performance in energy storage devices. Also, these graphene-particle hybrids (*e.g.*, graphene-copper nanoparticles (Cu/G)) can serve as advanced architectures for heterogeneous catalysis of CO_2 reduction and demonstrate superior catalytic properties over the carbon paper control and also pure Cu foil (Figure 6c).[87]

Crumpled GO microparticles have also been evaluated for their ability to absorb oil from aqueous solution and shown to outperform comparable activated carbon and carbon black particles.[96] Finally, crumpled graphene microparticles self-dispersed in oil were found to significantly improve the lubrication properties of polyalphaolefin base oil (Figure 6d).[97] In particular, even 0.01–0.1 wt.% of crumpled graphene particles remained self-dispersed and reduced the effective contact area, outperforming fully formulated commercial lubricants. Overall, the formation of crumpled particles from suspended 2D nanosheets represents a powerful approach for the creation of freestanding 3D graphene structures with core/shell architectures. Nevertheless, further work is needed to scale up these techniques, particularly in generating dispersed droplets and the significant energy cost of evaporating very dilute suspensions.

4. Folding (Origami) and Cutting (Kirigami) of 2D Materials

Origami can be understood as the shaping of a thin, inextensible sheet into a particular 3D geometry.[98] In particular, the difficulty of stretching 2D materials in-plane restricts how they can be manipulated into curved shapes. Intuitively, inextensible sheets (such as paper or aluminum foil) can be easily rolled and folded, but are challenging to shape into a dome. Mathematically, the curvature of a surface can be described by two principal curvatures C_1 and C_2, with a mean curvature $(C_1 + C_2)/2$ and an intrinsic (Gaussian) curvature (C_1C_2).[99] Continuous 2D material films are difficult to shape into domes with positive Gaussian curvature, since this would cause a divergent strain.[100] As an example, computational modeling of a graphene ribbon coated with a thin film of epoxy resin predicted that the composite would roll up cylindrically after annealing.[101] This global bending motion was driven by a thin coating of epoxy resin, which would chemically shrink and display mismatched thermal expansion with the graphene, resulting in one principal curvature that was extremely large ~0.14 nm^{-1}. Nevertheless, the Gaussian curvature remained zero, since the other principal curvature (along the axial direction) was zero. Another computational model investigated the localized folding of a graphene box with hydrogenated edges.[102] The hydrogenation of a given carbon atom resulted in a local lattice distortion, since the hydrogen attracts its bonded carbon atom while repelling its neighbors. A line of hydrogenated carbon atoms could result in localized bending of the graphene sheet. Folding of a graphene sheet into a box was shown to occur deterministically by applying an electric field to tune the intermolecular interactions, particularly the adhesion between layers.

Stimuli-responsive folding of multilayered GO was experimentally implemented by patterning localized regions of hydrophobicity.[103] A flat composite structure was patterned by sequentially filtering a GO solution, placing a stencil mask, then filtering additional GO-polydopamine (PDA) solution. Thus, the GO-PDA was spatially localized to specific regions of the topmost layers. Subsequent treatment with hydroiodic acid (HI) for reduction rendered the (unprotected) GO hydrophobic, while the (protected) PDA-GO regions remained hydrophilic. These grafted PDA-GO composite regions displayed increased propensity to adsorb (desorb) moisture, which resulted in swelling (shrinking) of the films, respectively, while the rGO regions were unresponsive to moisture. As a consequence of these spatially patterned material responses, the GO composite structure displayed localized actuations that resulted in larger scale shape changes. This actuation could also be triggered

by illumination with near infrared (NIR) light, which drove an increase in temperature and decrease in humidity within the GO composite. As a proof of concept, a freestanding microrobot was implemented that could walk and turn in response to light irradiation. Further, a self-folding box was demonstrated that could be triggered by NIR illumination for 2 second, then unfolded to a flat structure after illumination was halted (Figure 7a).

Kirigami augments origami by incorporating strategically located arrays of cutouts, which enables inextensible sheets to be shaped with non-zero Gaussian curvature.[104] Essentially, these cutouts define localized hinges that can undergo rotational motions to reduce strain. Kirigami was first demonstrated using a graphene monolayer prepared by a multistep fabrication process.[105] First, a graphene monolayer was transferred onto an aluminum-coated silicon wafer and photolithographically patterned to deposit gold pads. Cutouts were patterned in selected regions by brief treatment with oxygen plasma, after which the aluminum film was chemically etched to detach the graphene. The resulting freestanding structure could be manipulated with a computer-controlled micromanipulator attached to the gold pad. For instance, pulling the kirigami structure caused the graphene strands to pop out and deform out of plane (Figure 7b,c). These kirigami structures could undergo large strains, allowing the spring to be stretched over 240% without any degradation on the electrical properties (*i.e.*, conductance). The repeated stretching and relaxing the structure over 1000 cycles did not affect its electrical properties. Moreover, these structures could be remotely actuated by light or magnetic fields.

Kirigami has also been demonstrated in multilayered polymer-GO films, using a similar photolithographic patterning technique to selectively etch with oxygen plasma.[106] A different geometric patterns of cutouts was implemented with alternating lines or C-shapes (Figure 7d,e). Finite element modeling confirmed that the cutouts enabled hinge-like rotations that reduced the local stresses. These cutouts also enabled these films to undergo extremely large macroscopic strains without fracture, while retaining good electrical conductivity. This technique was further demonstrated with other materials, including polymer-carbon nanotube composites.

An evolution of this kirigami concept has recently been implemented with irregular geometric cuts to form nearly arbitrary 3D shapes,[107] in contrast with the regular geometric patterns of cutouts shown previously (*e.g.*, lattice kirigami).[108] In principle, these cutouts can also be utilized with 2D materials, provided that the freestanding film is homogeneous on length scales comparable to those of the cutouts. Conventional photolithography techniques have been shown to be particularly effective at selectively removing regions from a planar sheet with high spatial resolution. Nevertheless, further work will be needed to scale up kirigami cutouts beyond wafer scale. Moreover, as 2D materials are folded into increasingly complex configurations, misfolding and slow folding kinetics may need to be managed. These issues may potentially be addressed using concepts developed in material self-assembly, including external constraints and templating,[109] as well as computational modeling.[110]

5. 3D Printing with 2D Nanosheet Suspensions

Additive manufacturing ("3D printing") is emerging as a powerful route to engineered 3D microstructures, including well-defined periodic geometries. The resulting porous 3D structures exhibit functional properties that derive from the programmed geometric configuration of voids and solids as well as material composition.[111] The macroscopic properties of these structures are often dominated by the internal connectivity rather than the regularity of the microstructure. For instance, the mechanical deformation of a disordered "cellular" architecture found in foams or aerogels is governed by local bending, and results in a sharp decrease in stiffness as porosity decreases (scaling with relative density as ρ^2 for an open cell foam).[112] In general, more ordered lattice architectures can be advantageous since their mechanical deformation is governed by stretching, resulting in a linear dependence of stiffness on relative density.[113]

Graphene-based materials have potential as structural building blocks for some 3D printed technologies. Graphene-based carbon solids are electrically conductive, chemically inert, and can often be engineered for biocompatibility. Assembling nanosheets with preexisting sp^2-carbon networks allows formation of macroscopic carbon bodies without the very high-temperature processing required by other carbon material synthesis methods. This method also does not rely on creating or controlling out-of-plane deformation in individual nanosheets. Typically the pattern length scale in 3D printed objects in sufficiently large that a single nanosheet experiences a near-planar local environment. Thus unlike the previous examples, the fabrication challenge is the accurate delivery and deposition of nanosheets from engineered fluid phases rather than methods to systematically control nanosheet folding or wrinkling. To deposit a 3D structure with the desired geometry and composition, a computer-aided design is deconstructed into a particular sequence of motions, through which the nozzle (or sample) is spatially translated. This technique is highly sensitive to the viscoelastic properties of the ink, which has to satisfy several key design requirements. First, the ink should rapidly solidify once extruded from the nozzle. This can occur by formulating the ink to be shear thinning or to undergo rapid gelation in response to an applied stimulus. Second, the extruded ink must adhere to the previously deposited structure in order to form a continuous body. Finally, the solidified ink must be mechanically robust enough to maintain its shape under the load of the completed structure and the anticipated external stresses. Dilute aqueous suspensions of GO are ill-suited for direct ink writing, however, because they behave as low-viscosity Newtonian fluids.[114] Recent efforts have thus focused on careful engineering of the ink composition, rheological behaviors, and printing parameters to adjust the interactions between the 2D nanosheets in the printing suspension.

Several groups have recently demonstrated directed ink writing of GO by tuning the suspension viscoelasticity. One approach used GO nanosheets functionalized with a pH-sensitive branched copolymer surfactant (BCS) (Figure 8a).[115] At basic pH, the GO nanosheets remained dispersed due to electrostatic and steric repulsion from the BCS. As the pH of the GO/BCS ink decreased with the addition of gluconic-δ-lactone (GδL), multiple non-covalent interactions between BCS functional groups could take place, increasing the magnitude of the storage modulus to hold up the weight of these freestanding 3D objects (Figure 8b). Nevertheless, the weak forces of nanosheet association could be disrupted by

shear, permitting extrusion of the GO/BCS ink, followed by rapid gelation outside the nozzle. A second method added hydrophilic silica powders to a concentrated GO suspension in order to enhance shear thinning and increase viscosity (Figure 8c).[116] GO inks were printed into an isooctane bath which was immiscible with water, keeping the ink hydrated. Isooctane was also advantageous since it is less dense than water, providing additional mechanical support to the printed structure. In both these approaches, the 3D printed structure was subsequently freeze dried to remove water and annealed to reduce GO and decompose the BCS. Both structures displayed high electrical conductivity and recoverable elastomeric behaviors without compromising their periodic structure. The latter approach utilized an additional etching step to remove the silica, resulting in aerogel microstructures that were of extremely low density.

The addition of polymers to GO suspensions can further enhance the functionality of the printed structure. For instance, a GO ink was formulated using the biocompatible elastomer polylactide-co-glycolide (PLG) as a binding agent (Figure 8d).[117] This polymer-GO ink could be utilized under ambient conditions to print mechanically robust, flexible and electrically conductive scaffolds. These 3D printed structures were applied as a biomimetic scaffold to regulate cell adhesion, proliferation, and neurogenic differentiation. With this ease of fabrication, combined with the selection of printing materials, 3D printed graphene could be applied toward the design of a wide range of functional electronic, biological, and bioelectronic medical and nonmedical devices.

It may be desirable to remove these polymeric additives from the final 3D printed architecture in order to improve their structural and functional performance. However, pyrolysis of these polymers at high temperatures can often leave amorphous carbon residue, which can increase the electrical resistance and density of the printed structure. In order to print a lowviscosity GO suspension without binders or sacrificial additives, a hybrid freezing method was developed.[118] First, pure water was deposited onto a cooled surface (−25 C), which solidified into a rigid support structure of ice (Figure 8e). Next, GO ink droplets were dispersed onto the ice support structure. These liquid droplets partially melted the frozen support structure and intermixed, while filling in voids through surface tension and gravity. The deposited solution ultimately freezes and firmly bonds adjacent regions together. These structures underwent similar postprocessing by freeze drying to remove water, as well as thermal annealing. One advantage of this approach is intermixing of GO with the ice support structure results in further dilution, resulting in extremely low density aerogels (Figure 8e).

Beyond simple “logpile” geometries, 2D materials can potentially be integrated into rationally designed periodic architectures that do not exist naturally. These so-called “architectured metamaterials” display unnatural pore structures that enable extreme functionalities not observed at the continuum level.[119] Thus, the exceptional chemical and physical properties of 2D materials could be enhanced by their macroscopic configuration. For instance, 3D printed GO aerogels have been shown to be exceptionally lightweight structures with outstanding mechanical strength. Alternatively, multilayer graphene shows exceptional mechanical energy adsorption properties and could be utilized as protective armor against microprojectiles.[120] In principle, periodic architectures could be used to further dissipate and manipulate mechanical energy[121] or electromagnetic waves.[122]

Finally, these high surface area periodic architectures could be used to manipulate fluid transport for heat exchange and thermal management.[123] One limitation of direct ink writing techniques is that that the feature sizes are limited by nozzle diameter, typically on the order of hundreds of microns. Thus, there is some shear-driven alignment of 2D materials, but this process remains relatively uncontrolled. Finer and more complex geometries with higher resolution may be feasible through multiphoton lithography or other direct laser write techniques,[124] as well as alternative synthetic techniques to generate more anisotropic molecular ordering.[10,17]

6. Outlook: Heterostructures and 2D Materials Beyond Graphene

The pioneering work on graphene in 2004[125] inspired the search for other sheet-like structures, and that search has now produced an extensive library of 2D materials of widely varying chemistry.[126,127] These 2D materials “beyond graphene” can be regarded as a versatile tool kit to assemble higher dimensional architectures for a range of next-generation technologies.[128] In many cases, the synthesis, processing and characterization techniques previously developed for graphene may be applicable, which should accelerate technology development.[2,129] Major classes of 2D materials now include clays such as laponite and layered double hydroxides, transition metal oxides, transition metal dichalcogenides and hexagonal boron nitride (hBN).[130,131] Unlike graphene, many 2D materials have fundamental monolayers that consist of multiple (2–7) covalently bonded atomic planes, which increases mechanical stiffness and accommodates more complex chemistries. As a consequence, 2D materials can display a wide range of electronic properties, behaving as insulators, semiconductors and even superconductors. Thus, these alternative 2D materials can potentially circumvent some of the limitations of graphene as a zero band gap semiconductor.[132] For instance, water disinfection was recently demonstrated using vertically aligned molybdenum disulfide for the photocatalytic generation of reactive oxygen species (ROS).[133] The use of few layered sheets resulted in a direct bandgap of 1.55 eV, which was aligned with the visible light spectrum. Moreover, these nanostructured architectures increased the density of reaction sites while reducing the distance for electrons and holes to diffuse to the solid/liquid interface. The addition of copper or gold films further promoted catalysis and electron-hole pair separation to enhance ROS production. Overall, this device resulted in >99.999% inactivation of bacteria in 20 min with a small amount of material.

Programmed stacking of different 2D materials into heterostructures represents an exciting route towards designer crystal structures with tunable electronic and optical properties, analogous to molecular beam epitaxy.[134,135] Remarkably, these layered structures can be stabilized even by the relatively weak van-der-Waals interactions between 2D monolayers, acting in combination with the much stronger covalent in-plane bonding within each monolayer. As a consequence, these layered architectures can display atomically sharp interfaces without atomically matched or commensurate lattices. As an example, stacking of alternating titanate and zinc-chrome layered double hydroxides (Zn-Cr-LDH) into mesoporous architectures was utilized for photocatalytic production of hydrogen and oxygen gas from water.[136] The highly efficient photocatalytic activity under visible light illumination was enabled by the good physical contact and electronic coupling between the

layered components. There has also been substantial progress towards so-called van der Waals heterostructures, which display device characteristics based on programmed stacking sequences of monolayer or few layer building blocks.[137,138] These architectures can be laborious to prepare using transfer processes, and there has been increasing interest in direct synthesis.[139] An additional consideration is that these heterostructures are prone to surface contamination, which becomes trapped between layers. Finally, there has been exciting work to integrate of 2D materials with other nanomaterials of different dimensionality, including 0D nanocrystals and 1D nanowires, which may enable new structures and functions but also entail additional processing challenges.[140]

The high surface reactivity of 2D materials can be viewed as a useful feature for materials deposition, rather than as a nuisance that results in contamination. For instance, functionalized graphene or GO have often been used for the nucleation and growth of nanomaterials due to their rich surface chemistry, ease of aqueous processing, and enlarged interlayer gallery spaces.[141] By stacking GO sheets into multilayer films and introducing precursors through intercalation, the 2D interlayer gallery spaces can confine and guide the assembly and conversion of precursors into new 2D material structures after high-temperature calcination (Figure 9a). This concept has been first demonstrated using thick GO papers as intercalation templates to synthesize ZnO (Figure 9b),[142,143] TiO_2 (Figure 9c), Fe_2O_3 (Figure 9d), and $YBa_2Cu_3O_{7-\delta}$ (Y123) (Figure 9e)[144] lamellar structures in a planar configuration.

We have recently developed a new approach for creating hierarchically patterned metal oxide architectures using wrinkled and crumpled 3D graphene architectures as intercalation templates (Figure 9f).[145] For the first time, the complex topographical features can be transcribed into metal oxides, and even the finest structural features in multi-scale hierarchical GO templates can be replicated with high fidelity in ZnO, Al_2O_3, Mn_2O_3, and CuO films. This generalized approach introduces an indirect synthetic route for creating 2D metal oxides with crumple- and wrinkle-textures that cannot undergo the direct texturing by compression. We envision this intercalation templated synthesis will allow many of other graphene structures with higher dimensions to be replicated with a variety of other material compositions, even those that are unstable as 2D materials. More generally, direct (non-templating) processes for producing wrinkled or crumpled textures from 2D material building blocks beyond graphene remain largely unexplored. These 2D materials differ from graphene in that they can include multiple atomic layers, and the nanosheet building blocks prepared by exfoliation, colloidal, or solvothermal methods often have small lateral dimensions (< 200 nm). There exist tremendous opportunities to explore the phase space of higher dimensional architectures that can be fabricated with 2D materials, as well as to elucidate their mechanical behaviors. The recently reported oxidative degradation of transition metal dichalcogenides under ambient conditions[146,147] may also be a challenge for the long-term stability of such 3D structures. Alternatively, these degradation pathways may be an asset to be exploited for the creation of degradable scaffolds or removable templates.

Finally, the extreme confinement of molecular species within interlayer spacings can result in counterintuitive behaviors, including the formation of discrete molecular monolayers with

more solid-like or gas-like properties.[148–150] Recent measurements have revealed that these molecular species are under exceptionally large pressure due to large van der Waals interactions at small separations.[151] This high pressure (~1 GPa) is sufficient to trigger chemical reactions that would ordinarily occur with elevated temperature. As a consequence, several trapped salts such as $MgCl_2$, $CuSO_4$ and $Ca(OH_4)_2$ react with water to form 2D crystals of the corresponding metal oxides.[151] Thus, high dimensional patterning of 2D materials may facilitate new mechanochemical syntheses that are more energy efficient with reduced chemical waste.[152]

7. Summary

2D materials are ultrathin atomic crystals with extremely large surface area to volume ratios and novel physicochemical properties not observed in their parent 3D bulk materials. In this Progress Report, we discuss a selection of emerging methods for assembling and patterning 2D nanosheets into higher-dimensional architectures, which have been primarily inspired by graphene and GO. First, thin films of tiled 2D nanosheets can be wrinkled and/or crumpled with defined wavelength by mismatched mechanical deformation on soft elastomeric substrates. These textured surfaces can be reversibly unfolded under large deformations and have exciting applications as stretchable electronics and biomaterial interfaces. Second, 2D materials can be used to encapsulate microscale cargos with thin crumpled shells formed by isotropic compression during droplet drying. Crumpling prevents restacking and surface area loss chemically and mechanically robust in solution. Possible applications include nanoreactors, electrochemical reactors and lubricants. Third, 2D materials can be precisely shaped into complex 3D objects by folding (origami) and/or cutting (kirigami) operations, which permit local structural rotation to reduce strain. Cutouts in regular geometric patterns permit dome-like (Gaussian) curvature and large material deformations not achievable in space-filling films, and these have been utilized for folding boxes and freestanding microrobots. Fourth, 2D materials can be 3D-printed into regular lattice architectures through direct ink writing. The required liquid phase extrusion from a nozzle requires careful optimization of the nanosheet suspension rheology, often through the addition of polymers or other binding agents. Macroporous 3D printed architectures have been demonstrated as ultralow density materials and as scaffolds for neuronal tissue engineering. Finally, 2D materials can be vertically stacked as van der Waals heterostructures, displaying atomically layered architectures with electronic and optically coupled behaviors. Their interlayer spacings can also be used as templates to assemble new materials in 2D confinement. By combining this templating concept with the first texturing technique described above (compressive wrinkling), one can fabricate textured metal oxide films that replicate the original features created by graphene wrinkling. Common to all these examples is that the shaping of 2D materials is governed by out-of-plane bending relative to in-plane stretching. In all cases, intermolecular and surface interactions involving 2D nanosheets and surrounding fluid phases play a critical role in assembly. Traditionally, coating processes have been optimized for the controlled manipulation of particulate solutions, with particular consideration of interfacial rheology.[153] These concepts may facilitate conformal deposition of 2D materials on large-area or nonplanar substrates through spray deposition.[154,155] Although these techniques were initially demonstrated with graphene

and GO, we envision they should be broadly applicable for a wide variety of 2D materials beyond graphene.

Overall, these physicochemical concepts have motivated the development of innovative fabrication techniques that may be scalable beyond wafer sizes, curved and complex geometries, as well as for unconventional materials, although considerable refinement is still necessary prior to commercial use.[1] Non-planar geometries are particularly useful for electrochemical applications in energy storage and biosensing, since the increased surface areas may enhance electrode-electrolyte interactions as well as decreasing path lengths for transport. Most previous studies have focused on graphene materials and there is tremendous potential to extend the field to the broader set of inorganic 2D materials. There now exists a widely available library of nanosheet building blocks, but these have not yet been systematically exploited using the 3D patterning techniques discussed here. In the future, we anticipate that higher dimensional architectures built from a diverse set of 2D nanosheet building blocks will enable important fundamental and applied advances in advanced materials, energy storage and conversion, as well as biomedical and environmental technologies.

Acknowledgments

We apologize to colleagues whose work could not be covered due to space limitations. We thank K. S. Kim and V. L. Colvin for helpful discussions. This work was supported by the Hibbitt Engineering Postdoctoral Fellowship, an OVPR Research Seed Award from Brown University, NSF INSPIRE grant CBET-1344097 and the NIEHS Superfund Research Program P42-ES013660.

Biographies

Po-Yen Chen is an Hibbitt Engineering Postdoctoral Fellow at Brown University. He previously completed his Ph.D. in Chemical Engineering from Massachusetts Institute of Technology. His research interests include the self-assembly of nanomaterial building blocks, higher dimensional patterning of 2D materials, as well as the templated synthesis of nanocomposites for energy conversion and storage devices.

Robert H. Hurt is Professor of Engineering at Brown University. He holds degrees in Chemical Engineering from Michigan Tech (B.S.) and MIT (Ph.D.) and held prior posts at Bayer AG and Sandia National Laboratories. He was the Founding Director of the Institute for Molecular and Nanoscale Innovation at Brown, and is currently the Editor-in-Chief of *Carbon* and Director of Brown's NIH Superfund Research Center. His current research focuses on 2D materials, environmental nanotechnology, nanotoxicology and safe design, and the use of graphene as a building block for new 3D material architectures.

Ian Y. Wong is an Assistant Professor of Engineering and of Medical Science at Brown University. He completed his Ph.D. in Materials Science & Engineering from Stanford University and postdoctoral training in Biomedical Engineering at Massachusetts General Hospital and Harvard Medical School. His research interests include the self-organization and additive manufacturing of 2D materials, fundamental cell-material interactions, as well as the development and characterization of microfluidic biomaterials for cancer biology.

References

1. Ferrari AC, Bonaccorso F, Fal'ko V, Novoselov KS, Roche S, Bøggild P, Borini S, Koppens FHL, Palermo V, Pugno N, Garrido JA, Sordan R, Bianco A, Ballerini L, Prato M, Lidorikis E, Kivioja J, Marinelli C, Ryhanen T, Morpurgo A, Coleman JN, Nicolosi V, Colombo L, Fert A, Garcia-Hernandez M, Bachtold A, Schneider GF, Guinea F, Dekker C, Barbone M, Sun Z, Galiotis C, Grigorenko AN, Konstantatos G, Kis A, Katsnelson M, Vandersypen L, Loiseau A, Morandi V, Neumaier D, Treossi E, Pellegrini V, Polini M, Tredicucci A, Williams GM, Hee Hong B, Ahn J-H, Min Kim J, Zirath H, van Wees BJ, van der Zant H, Occhipinti L, Di Matteo A, Kinloch IA, Seyller T, Quesnel E, Feng X, Teo K, Rupesinghe N, Hakonen P, Neil SRT, Tannock Q, Löfwander T, Kinaret J. Nanoscale. 2015; 7:4598. [PubMed: 25707682]
2. Butler SZ, Hollen SM, Cao L, Cui Y, Gupta JA, Gutiérrez HR, Heinz TF, Hong SS, Huang J, Ismach AF, Johnston-Halperin E, Kuno M, Plashnitsa VV, Robinson RD, Ruoff RS, Salahuddin S, Shan J, Shi L, Spencer MG, Terrones M, Windl W, Goldberger JE. ACS Nano. 2013; 7:2898. [PubMed: 23464873]
3. Novoselov KS, Falko VI, Colombo L, Gellert PR, Schwab MG, Kim K. Nature. 2012; 490:192. [PubMed: 23060189]
4. Geim AK, Grigorieva IV. Nature. 2013; 499:419. [PubMed: 23887427]
5. Rogers, JA., Lee, HH. Unconventional Nanopatterning Techniques and Applications. John Wiley & Sons; 2008.
6. Wassei JK, Kaner RB. Acc. Chem. Res. 2013; 46:2244. [PubMed: 23305347]
7. Park S, Ruoff RS. Nat. Nano. 2009; 4:217.
8. Parviz D, Irin F, Shah SA, Das S, Sweeney CB, Green MJ. Adv. Mater. 2016:1.
9. Whitby RLD. ACS Nano. 2014; 8:9733. [PubMed: 25244511]
10. Kim J, Cote LJ, Huang J. Acc. Chem. Res. 2012; 45:1356. [PubMed: 22663082]
11. Gudarzi MM. Langmuir. 2016; 32:5058. [PubMed: 27143102]
12. Konkena B, Vasudevan S. J. Phys. Chem. C. 2014; 118:21706.
13. Cote LJ, Kim J, Zhang Z, Sun C, Huang J. Soft Matter. 2010; 6:6096.
14. Woltornist SJ, Oyer AJ, Carrillo J-MY, Dobrynin AV, Adamson DH. ACS Nano. 2013; 7:7062. [PubMed: 23879536]
15. Xu Z, Gao C. ACS Nano. 2011; 5:2908. [PubMed: 21375309]
16. Guo F, Kim F, Han TH, Shenoy VB, Huang J, Hurt RH. ACS Nano. 2011; 5:8019. [PubMed: 21877716]
17. Narayan R, Kim JE, Kim JY, Lee KE, Kim SO. Adv. Mater. 2016; 28:3045. [PubMed: 26928388]
18. Dikin DA, Stankovich S, Zimney EJ, Piner RD, Dommett GHB, Evmenenko G, Nguyen ST, Ruoff RS. Nature. 2007; 448:457. [PubMed: 17653188]
19. Berry V. Carbon. 2013; 62:1.
20. Goh K, Karahan HE, Wei L, Bae T-H, Fane AG, Wang R, Chen Y. Carbon. 2016; 109:694.
21. Mukherjee R, Thomas AV, Krishnamurthy A, Koratkar N. ACS Nano. 2012; 6:7867. [PubMed: 22881216]
22. Jin Z, Lu W, O'Neill KJ, Parilla PA, Simpson LJ, Kittrell C, Tour JM. Chem. Mater. 2011; 23:923.
23. Guo F, Creighton M, Chen Y, Hurt R, Külaots I. Carbon. 2014; 66:476. [PubMed: 26478597]
24. Joshi RK, Carbone P, Wang FC, Kravets VG, Su Y, Grigorieva IV, Wu HA, Geim AK, Nair RR. Science. 2014; 343:752. [PubMed: 24531966]
25. Maiti UN, Lim J, Lee KE, Lee WJ, Kim SO. Adv. Mater. 2014; 26:615. [PubMed: 24136778]
26. Bai H, Li C, Wang X, Shi G. Chem. Commun. 2010; 46:2376.
27. Ai W, Du Z-Z, Liu J-Q, Zhao F, Yi M-D, Xie L-H, Shi N-E, Ma Y-W, Qian Y, Fan Q-L, Yu T, Huang W. RSC Adv. 2012; 2:12204.
28. Zhang X, Sui Z, Xu B, Yue S, Luo Y, Zhan W, Liu B. J. Mater. Chem. 2011; 21:6494.
29. Pham HD, Pham VH, Cuong TV, Nguyen-Phan T-D, Chung JS, Shin EW, Kim S. Chem. Commun. 2011; 47:9672.

30. Wu Z-S, Pei S, Ren W, Tang D, Gao L, Liu B, Li F, Liu C, Cheng H-M. Adv. Mater. 2009; 21:1756.
31. Huang S-Y, Wu G-P, Chen C-M, Yang Y, Zhang S-C, Lu C-X. Carbon. 2013; 52:613.
32. Chen Y, Zhang X, Yu P, Ma Y. J. Power Sources. 2010; 195:3031.
33. Chen Z, Ren W, Gao L, Liu B, Pei S, Cheng H-M. Nat. Mater. 2011; 10:424. [PubMed: 21478883]
34. Yang Z, Yan C, Liu J, Chabi S, Xia Y, Zhu Y. RSC Adv. 2015; 5:29397.
35. Woltornist SJ, Carrillo J-MY, Xu TO, Dobrynin AV, Adamson DH. Macromolecules. 2015; 48:687.
36. Nishihara H, Yang Q-H, Hou P-X, Unno M, Yamauchi S, Saito R, Paredes JI, Martínez-Alonso A, Tascón JMD, Sato Y, Terauchi M, Kyotani T. Carbon. 2009; 47:1220.
37. Sherrell PC, Mattevi C. Mater. Today. 2016
38. Raccichini R, Varzi A, Passerini S, Scrosati B. Nat. Mater. 2015; 14:271. [PubMed: 25532074]
39. Perreault F, Fonseca de Faria A, Elimelech M. Chem. Soc. Rev. 2015; 44:5861. [PubMed: 25812036]
40. Deng D, Novoselov KS, Fu Q, Zheng N, Tian Z, Bao X. Nat. Nano. 2016; 11:218.
41. Chen Z, Dong L, Yang D, Lu H. Adv. Mater. 2013; 25:5352. [PubMed: 24089354]
42. Kurapati R, Kostarelos K, Prato M, Bianco A. Adv. Mater. 2016; 28:6052. [PubMed: 27105929]
43. Lee C, Wei X, Kysar JW, Hone J. Science. 2008; 321:385. [PubMed: 18635798]
44. Meyer JC, Geim AK, Katsnelson MI, Novoselov KS, Booth TJ, Roth S. Nature. 2007; 446:60. [PubMed: 17330039]
45. Deng S, Berry V. Mater. Today. 2016; 19:197.
46. Zang J, Ryu S, Pugno N, Wang Q, Tu Q, Buehler MJ, Zhao X. Nat. Mater. 2013; 12:321. [PubMed: 23334002]
47. Xu P, Kang J, Choi J-B, Suhr J, Yu J, Li F, Byun J-H, Kim B-S, Chou T-W. ACS Nano. 2014; 8:9437. [PubMed: 25144124]
48. Wang Z, Tonderys D, Leggett SE, Williams EK, Kiani MT, Spitz Steinberg R, Qiu Y, Wong IY, Hurt RH. Carbon. 2016; 97:14. [PubMed: 25848137]
49. Thomas AV, Andow BC, Suresh S, Eksik O, Yin J, Dyson AH, Koratkar N. Adv. Funct. Mater. 2015; 27:3256.
50. Zang J, Cao C, Feng Y, Liu J, Zhao X. Sci. Rep. 2014; 4:6492. [PubMed: 25270673]
51. Sun J-Y, Xia S, Moon M-W, Oh KH, Kim K-S. Proc. R. Soc. A. 2011
52. Shield TW, Kim KS, Shield RT. J. Appl. Mech. 1994; 61:231.
53. Zhao R, Zhang T, Diab M, Gao H, Kim KS. Extreme Mech. Lett. 2015; 4:76.
54. Huang ZY, Hong W, Suo Z. J. Mech. Phys. Solids. 2005; 53:2101.
55. Cao Y, Hutchinson JW. J. Appl. Mech. 2012; 79:031019.
56. Wang Q, Zhao X. Sci. Rep. 2015; 5:8887. [PubMed: 25748825]
57. Lin S, Lee EK, Nguyen N, Khine M. Lab Chip. 2014; 14:3475. [PubMed: 25075652]
58. Zhang B, Cui T. 2012 IEEE 25th International Conference on Micro Electro Mechanical Systems (MEMS). 2012:1360.
59. Wang MC, Chun S, Han RS, Ashraf A, Kang P, Nam S. Nano Lett. 2015; 15:1829. [PubMed: 25667959]
60. Chen P-Y, Sodhi J, Qiu Y, Valentin TM, Steinberg RS, Wang Z, Hurt RH, Wong IY. Adv. Mater. 2016; 28:3564. [PubMed: 26996525]
61. Chen T, Dai L. Mater. Today. 2013; 16:272.
62. Bruce PG, Scrosati B, Tarascon J-M. Angew. Chem. Int. Ed. 2008; 47:2930.
63. Soleymani L, Fang Z, Sargent EH, Kelley SO. Nat. Nano. 2009; 4:844.
64. Kim JY, Lim J, Jin HM, Kim BH, Jeong S-J, Choi DS, Li DJ, Kim SO. Adv. Mater. 2016; 28:1591. [PubMed: 26660004]
65. Kang P, Wang MC, Knapp PM, Nam S. Adv. Mater. 2016; 28:4639. [PubMed: 27061899]
66. Leem J, Wang MC, Kang P, Nam S. Nano Lett. 2015; 15:7684. [PubMed: 26501429]
67. Rosset S, Shea HR. Appl. Phys. A. 2013; 110:281.

68. Feng C, Yi Z, Dumée LF, Garvey CJ, She F, Lin B, Lucas S, Schütz J, Gao W, Peng Z, Kong L. Carbon. 2015; 93:878.
69. Curtis A, Wilkinson C. Biomaterials. 1997; 18:1573. [PubMed: 9613804]
70. Sanchez VC, Jachak A, Hurt RH, Kane AB. Chem. Res. Toxicol. 2012; 25:15. [PubMed: 21954945]
71. Kim D-H, Lu N, Huang Y, Rogers JA. MRS Bull. 2012; 37:226.
72. Ghosh, SK. Functional Coatings: by Polymer Microencapsulation. John Wiley & Sons; 2006.
73. Guo F, Silverberg G, Bowers S, Kim S-P, Datta D, Shenoy V, Hurt RH. Environ. Sci. Technol. 2012; 46:7717. [PubMed: 22717015]
74. Su Y, Kravets VG, Wong SL, Waters J, Geim AK, Nair RR. Nat. Commun. 2014; 5
75. Creighton MA, Zhu W, van Krieken F, Petteruti RA, Gao H, Hurt RH. ACS Nano. 2016; 10:2268. [PubMed: 26775824]
76. Chen X, Yin J. Soft Matter. 2010; 6:5667.
77. Gomes MAF. J. Phys. A: Math. Gen. 1987; 20:L283.
78. Luo J, Jang HD, Sun T, Xiao L, He Z, Katsoulidis AP, Kanatzidis MG, Gibson JM, Huang J. ACS Nano. 2011; 5:8943. [PubMed: 21995602]
79. Vliegenthart GA, Gompper G. Nat. Mater. 2006; 5:216. [PubMed: 16462740]
80. Bunch JS, Verbridge SS, Alden JS, van der Zande AM, Parpia JM, Craighead HG, McEuen PL. Nano Lett. 2008; 8:2458. [PubMed: 18630972]
81. Ma X, Zachariah MR, Zangmeister CD. Nano Lett. 2012; 12:486. [PubMed: 22185469]
82. Wang W-N, Jiang Y, Biswas P. J. Phys. Chem. Lett. 2012; 3:3228. [PubMed: 26296034]
83. Parviz D, Metzler SD, Das S, Irin F, Green MJ. Small. 2015; 11:2661. [PubMed: 25641827]
84. Zangmeister CD, Ma X, Zachariah MR. Chem. Mater. 2012; 24:2554.
85. Chen Y, Guo F, Jachak A, Kim S-P, Datta D, Liu J, Kulaots I, Vaslet C, Jang HD, Huang J, Kane A, Shenoy VB, Hurt RH. Nano Lett. 2012; 12:1996. [PubMed: 22429091]
86. Mao S, Wen Z, Kim H, Lu G, Hurley P, Chen J. ACS Nano. 2012; 6:7505. [PubMed: 22838735]
87. Wang Z, Lv X, Chen Y, Liu D, Xu X, Palmore GTR, Hurt RH. Nanoscale. 2015; 7:10267. [PubMed: 25992964]
88. Lee JY, Lee K-H, Kim YJ, Ha JS, Lee S-S, Son JG. Adv. Funct. Mater. 2015; 25:3606.
89. Han TH, Lee WJ, Lee DH, Kim JE, Choi E-Y, Kim SO. Adv. Mater. 2010; 22:2060. [PubMed: 20352629]
90. Yoon Y, Lee K, Baik C, Yoo H, Min M, Park Y, Lee SM, Lee H. Adv. Mater. 2013; 25:4437. [PubMed: 23788264]
91. Sun Y, Liu N, Cui Y. Nat. Energy. 2016; 1:16071.
92. Luo J, Jang HD, Huang J. ACS Nano. 2013; 7:1464. [PubMed: 23350607]
93. Mao S, Wen Z, Huang T, Hou Y, Chen J. Energy Environ. Sci. 2014; 7:609.
94. Lee WJ, Hwang TH, Hwang JO, Kim HW, Lim J, Jeong HY, Shim J, Han TH, Kim JY, Choi JW, Kim SO. Energy Environ. Sci. 2014; 7:621.
95. Luo J, Zhao X, Wu J, Jang HD, Kung HH, Huang J. J. Phys. Chem. Lett. 2012; 3:1824. [PubMed: 26291867]
96. Sohn K, Joo Na Y, Chang H, Roh K-M, Dong Jang H, Huang J. Chem. Commun. 2012; 48:5968.
97. Dou X, Koltonow AR, He X, Jang HD, Wang Q, Chung Y-W, Huang J. Proc. Natl. Acad. Sci. 2016; 113:1528. [PubMed: 26811466]
98. O'Rourke, J. How to Fold It: The Mathematics of Linkages, Prigami, and Polyhedra. Cambridge University Press; 2011.
99. Kamien RD. Rev. Mod. Phys. 2002; 74:953.
100. Witten TA. Rev. Mod. Phys. 2007; 79:643.
101. Li C, Koslowski M, Strachan A. Nano Lett. 2014; 14:7085. [PubMed: 25375290]
102. Zhu S, Li T. ACS Nano. 2014; 8:2864. [PubMed: 24564284]
103. Mu J, Hou C, Wang H, Li Y, Zhang Q, Zhu M. Sci. Adv. 2015; 1
104. Yang S, Choi I-S, Kamien RD. MRS Bull. 2016; 41:130.

105. Blees MK, Barnard AW, Rose PA, Roberts SP, McGill KL, Huang PY, Ruyack AR, Kevek JW, Kobrin B, Muller DA, McEuen PL. Nature. 2015; 524:204. [PubMed: 26222025]
106. Shyu TC, Damasceno PF, Dodd PM, Lamoureux A, Xu L, Shlian M, Shtein M, Glotzer SC, Kotov NA. Nat. Mater. 2015; 14:785. [PubMed: 26099109]
107. Zhang Y, Yan Z, Nan K, Xiao D, Liu Y, Luan H, Fu H, Wang X, Yang Q, Wang J, Ren W, Si H, Liu F, Yang L, Li H, Wang J, Guo X, Luo H, Wang L, Huang Y, Rogers JA. Proc. Natl. Acad. Sci. 2015; 112:11757. [PubMed: 26372959]
108. Sussman DM, Cho Y, Castle T, Gong X, Jung E, Yang S, Kamien RD. Proc. Natl. Acad. Sci. 2015; 112:7449. [PubMed: 26015582]
109. Whitesides GM, Boncheva M. Proc. Natl. Acad. Sci. 2002; 99:4769. [PubMed: 11959929]
110. Hawkes E, An B, Benbernou NM, Tanaka H, Kim S, Demaine ED, Rus D, Wood RJ. Proc. Natl. Acad. Sci. 2010; 107:12441. [PubMed: 20616049]
111. Gibson, L., Ashby, M. Cellular Solids: Structure and Properties. Cambridge: 1999.
112. Deshpande VS, Ashby MF, Fleck NA. Acta Mater. 2001; 49:1035.
113. Fleck NA, Deshpande VS, Ashby MF. Proc. R. Soc. A. 2010; 466:2495.
114. Naficy S, Jalili R, Aboutalebi SH, Gorkin RA Iii, Konstantinov K, Innis PC, Spinks GM, Poulin P, Wallace GG. Mater. Horiz. 2014; 1:326.
115. García-Tuñon E, Barg S, Franco J, Bell R, Eslava S, D'Elia E, Maher RC, Guitian F, Saiz E. Adv. Mater. 2015; 27:1688. [PubMed: 25605024]
116. Zhu C, Han TY-J, Duoss EB, Golobic AM, Kuntz JD, Spadaccini CM, Worsley MA. Nat. Commun. 2015; 6
117. Jakus AE, Secor EB, Rutz AL, Jordan SW, Hersam MC, Shah RN. ACS Nano. 2015; 9:4636. [PubMed: 25858670]
118. Zhang Q, Zhang F, Medarametla SP, Li H, Zhou C, Lin D. Small. 2016; 12:1702. [PubMed: 26861680]
119. Schaedler TA, Carter WB. Annu. Rev. Mater. Res. 2016; 46:187.
120. Lee J-H, Loya PE, Lou J, Thomas EL. Science. 2014; 346:1092. [PubMed: 25430764]
121. Lee J-H, Singer JP, Thomas EL. Adv. Mater. 2012; 24:4782. [PubMed: 22899377]
122. Liu Y, Zhang X. Chem. Soc. Rev. 2011; 40:2494. [PubMed: 21234491]
123. Roper CS, Schubert RC, Maloney KJ, Page D, Ro CJ, Yang SS, Jacobsen AJ. Adv. Funct. Mater. 2015; 27:2479.
124. LaFratta CN, Fourkas JT, Baldacchini T, Farrer RA. Angew. Chem. Int. Ed. 2007; 46:6238.
125. Novoselov KS, Geim AK, Morozov SV, Jiang D, Zhang Y, Dubonos SV, Grigorieva IV, Firsov AA. Science. 2004; 306:666. [PubMed: 15499015]
126. Mas-Balleste R, Gomez-Navarro C, Gomez-Herrero J, Zamora F. Nanoscale. 2011; 3:20. [PubMed: 20844797]
127. Novoselov KS, Jiang D, Schedin F, Booth TJ, Khotkevich VV, Morozov SV, Geim AK. Proc. Natl. Acad. Sci. 2005; 102:10451. [PubMed: 16027370]
128. Zhang X, Hou L, Ciesielski A, Samorì P. Adv. Energy Mater. 2016 n/a.
129. Ciesielski A, Samorì P. Adv. Mater. 2016; 28:6030. [PubMed: 26928750]
130. Bhimanapati GR, Lin Z, Meunier V, Jung Y, Cha J, Das S, Xiao D, Son Y, Strano MS, Cooper VR, Liang L, Louie SG, Ringe E, Zhou W, Kim SS, Naik RR, Sumpter BG, Terrones H, Xia F, Wang Y, Zhu J, Akinwande D, Alem N, Schuller JA, Schaak RE, Terrones M, Robinson JA. ACS Nano. 2015; 9:11509. [PubMed: 26544756]
131. Gupta A, Sakthivel T, Seal S. Prog. Mater. Sci. 2015; 73:44.
132. Algara-Siller G, Severin N, Chong SY, Björkman T, Palgrave RG, Laybourn A, Antonietti M, Khimyak YZ, Krasheninnikov AV, Rabe JP, Kaiser U, Cooper AI, Thomas A, Bojdys MJ. Angew. Chem. Int. Ed. 2014; 53:7450.
133. Liu C, Kong D, Hsu P-C, Yuan H, Lee H-W, Liu Y, Wang H, Wang S, Yan K, Lin D, Maraccini PA, Parker KM, Boehm AB, Cui Y. Nat. Nano. 2016 In Press.
134. Jariwala D, Marks TJ, Hersam MC. Nat. Mater. 2016 In Press.
135. Wang X, Xia F. Nat. Mater. 2015; 14:264. [PubMed: 25643031]

136. Gunjakar JL, Kim TW, Kim HN, Kim IY, Hwang S-J. J. Am. Chem. Soc. 2011; 133:14998. [PubMed: 21861530]
137. Lee C-H, Lee G-H, van der Zande AM, Chen W, Li Y, Han M, Cui X, Arefe G, Nuckolls C, Heinz TF, Guo J, Hone J, Kim P. Nat. Nano. 2014; 9:676.
138. Gong Y, Lin J, Wang X, Shi G, Lei S, Lin Z, Zou X, Ye G, Vajtai R, Yakobson BI, Terrones H, Terrones M, Tay Beng K, Lou J, Pantelides ST, Liu Z, Zhou W, Ajayan PM. Nat. Mater. 2014; 13:1135. [PubMed: 25262094]
139. Lin Y-C, Lu N, Perea-Lopez N, Li J, Lin Z, Peng X, Lee CH, Sun C, Calderin L, Browning PN, Bresnehan MS, Kim MJ, Mayer TS, Terrones M, Robinson JA. ACS Nano. 2014; 8:3715. [PubMed: 24641706]
140. Jariwala D, Sangwan VK, Wu C-C, Prabhumirashi PL, Geier ML, Marks TJ, Lauhon LJ, Hersam MC. Proc. Natl. Acad. Sci. 2013; 110:18076. [PubMed: 24145425]
141. Li Z, Wu S, Lv W, Shao J-J, Kang F, Yang Q-H. Small. 2016; 12:2674. [PubMed: 27059262]
142. Yeh C-N, Raidongia K, Shao J, Yang Q-H, Huang J. Nat. Chem. 2015; 7:166.
143. Saito Y, Luo X, Zhao C, Pan W, Chen C, Gong J, Matsumoto H, Yao J, Wu H. Adv. Funct. Mater. 2015; 25:5683.
144. Boston R, Bell A, Ting VP, Rhead AT, Nakayama T, Faul CFJ, Hall SR. CrystEngComm. 2015; 17:6094.
145. Chen P-Y, Liu M, Valentin TM, Wang Z, Spitz Steinberg R, Sodhi J, Wong IY, Hurt RH. ACS Nano. 2016; doi: 10.1021/acsnano.6b05179
146. Gao J, Li B, Tan J, Chow P, Lu T-M, Koratkar N. ACS Nano. 2016; 10:2628. [PubMed: 26808328]
147. Wang Z, von dem Bussche A, Qiu Y, Valentin TM, Gion K, Kane AB, Hurt RH. Environ. Sci. Technol. 2016; 50:7208. [PubMed: 27267956]
148. Xu K, Cao P, Heath JR. Science. 2010; 329:1188. [PubMed: 20813950]
149. Cao P, Xu K, Varghese JO, Heath JR. Nano Lett. 2011; 11:5581. [PubMed: 22050080]
150. Algara-Siller G, Lehtinen O, Wang FC, Nair RR, Kaiser U, Wu HA, Geim AK, Grigorieva IV. Nature. 2015; 519:443. [PubMed: 25810206]
151. Vasu KS, Prestat E, Abraham J, Dix J, Kashtiban RJ, Beheshtian J, Sloan J, Carbone P, Neek-Amal M, Haigh SJ, Geim AK, Nair RR. Nat. Commun. 2016; 7
152. Balaz P, Achimovicova M, Balaz M, Billik P, Cherkezova-Zheleva Z, Criado JM, Delogu F, Dutkova E, Gaffet E, Gotor FJ, Kumar R, Mitov I, Rojac T, Senna M, Streletskii A, Wieczorek-Ciurowa K. Chem. Soc. Rev. 2013; 42:7571. [PubMed: 23558752]
153. Cohen, ED., Gutoff, EB. Modern Coating and Drying Technology. Wiley-VCH; 1992.
154. Peter L, Umar K, Andrew H, Iftikhar A, Jonathan NC. Mater. Res. Express. 2016; 3:035007.
155. Kelly AG, Finn D, Harvey A, Hallam T, Coleman JN. Appl. Phys. Lett. 2016; 109:023107.

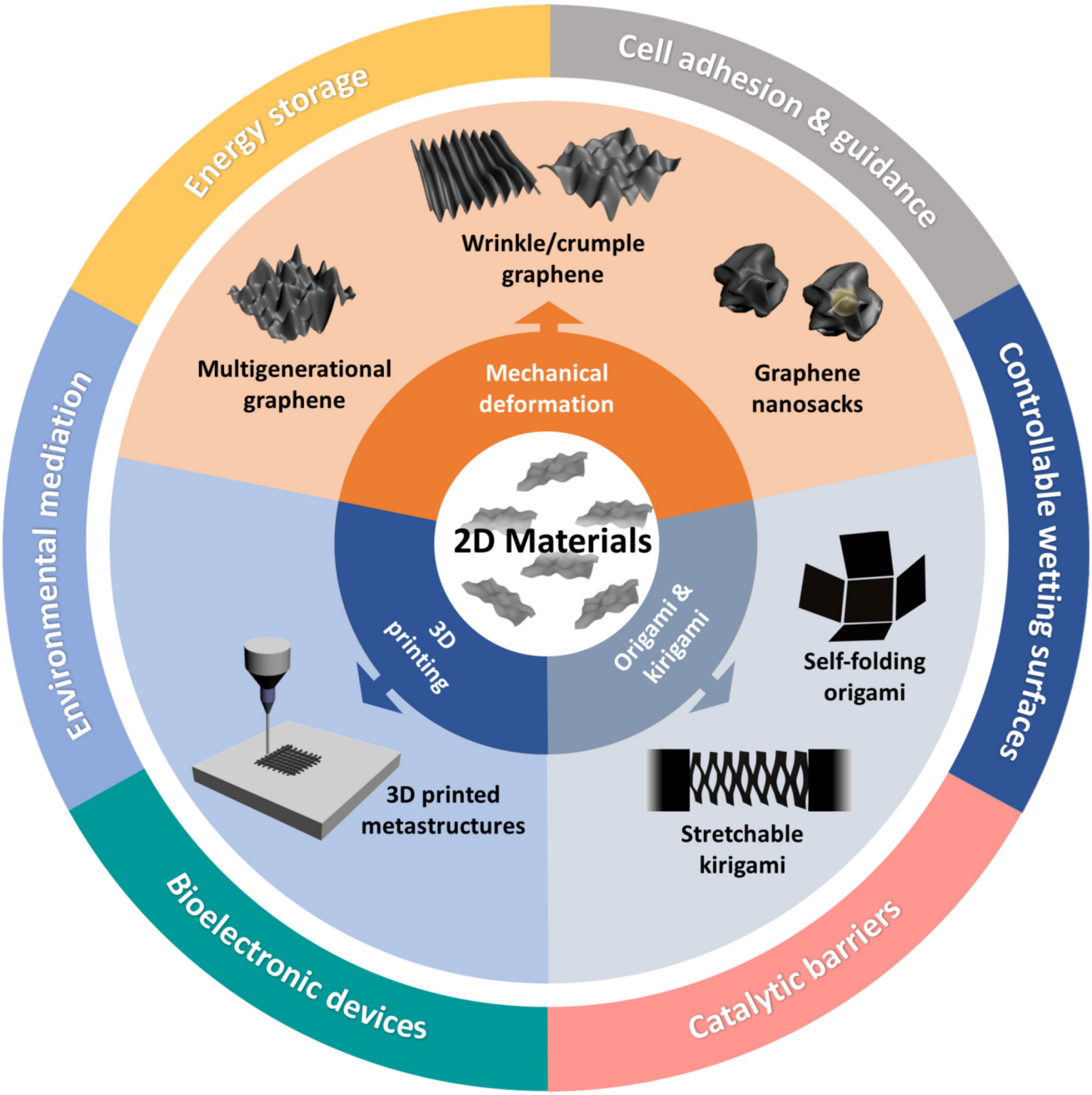

Figure 1. Schematic Summary

Creation methods of higher-dimensional 2D materials and the multifunctionality of resulting surface patterns in various technological applications.

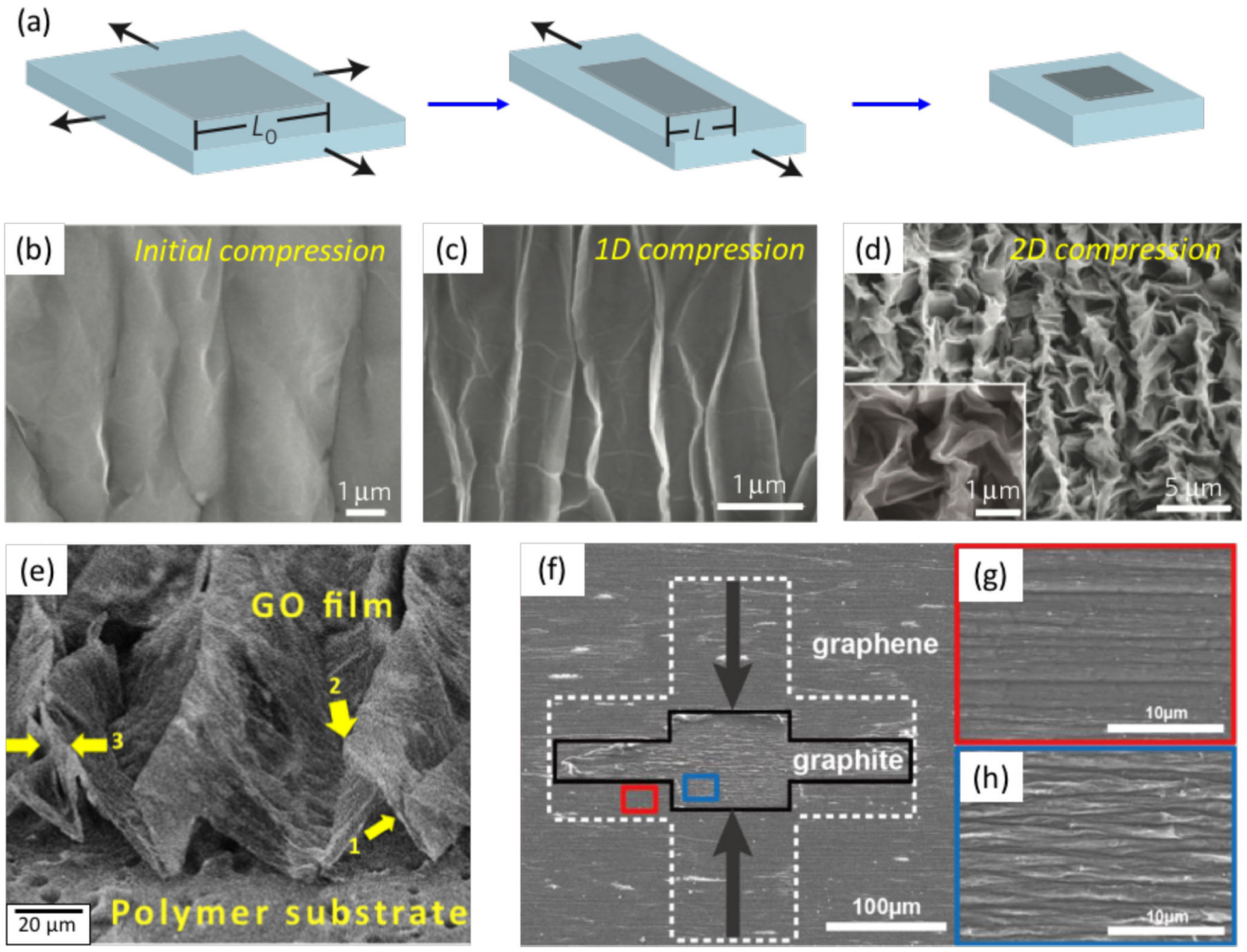

Figure 2. Wrinkled and crumpled surface patterns created by mechanical deformation

(a) Schematic illustration shows how microscopic patterns of 2D materials (*e.g.*, graphene) are fabricated via mismatched mechanical deformation.[46] (b) The SEM image shows the flat surface morphology of graphene paper at initial compression.[46] (c),(d) As the elastomeric substrate is deformed uniaxially or biaxially, the graphene film exhibits periodic wrinkles and disordered crumples, respectively.[46] Reproduced with permission from ref. 46. Copyright 2013, Nature Publishing Group. (e) SEM images of delaminated wrinkles with vertical ridges via uniaxial mechanical deformation.[48] Reproduced with permission[48] from ref. 48. Copyright 2016, Elsevier. (f) Heterogeneous uniaxial wrinkles via local heating. SEM image of heterogeneous graphene/graphite cross pattern subjected to 70% uniaxial strain.[59] (g) Thin graphene outside the cross pattern exhibits smaller wrinkles.[59] (h) Thick graphite inside the cross pattern present larger wrinkling features.[59] Reproduced with permission from ref. 59. Copyright 2015 American Chemical Society.

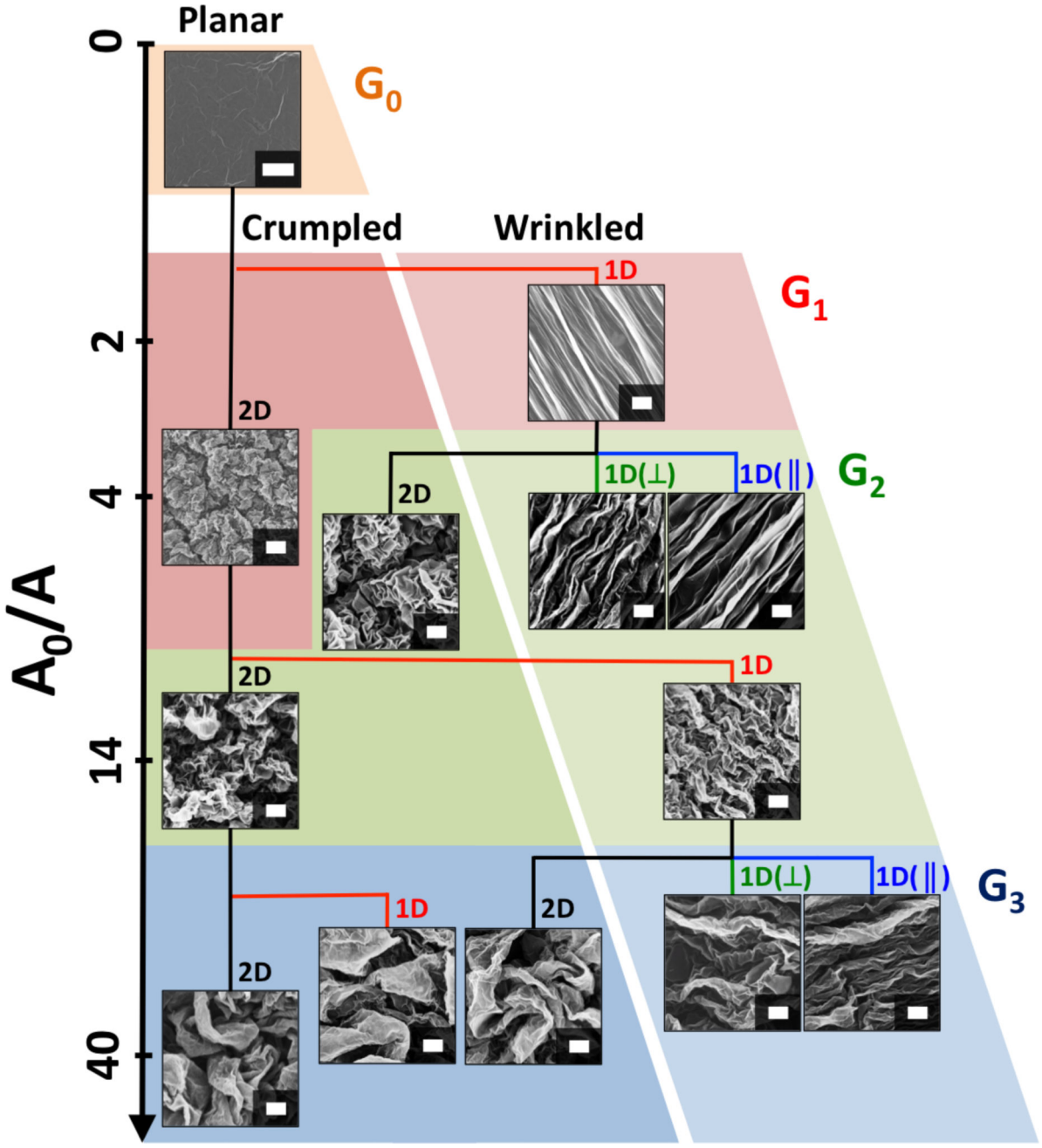

Figure 3. Sequential deformation for the fabrication of multigenerational GO structures

The genealogy of multigenerational GO structures from planar coatings (G_1) to multiscale structures (G_1–G_3). A_0 indicates the area of initial planar film; A is the area of multigenerational GO film. Scale bar in the SEM of G_0 coating is 10 μm, and scale bars in G_1, G_2, G_3 SEM images are all 4 μm.[60] Reproduced with permission from ref. 60. Copyright 2016, Wiley-VCH.

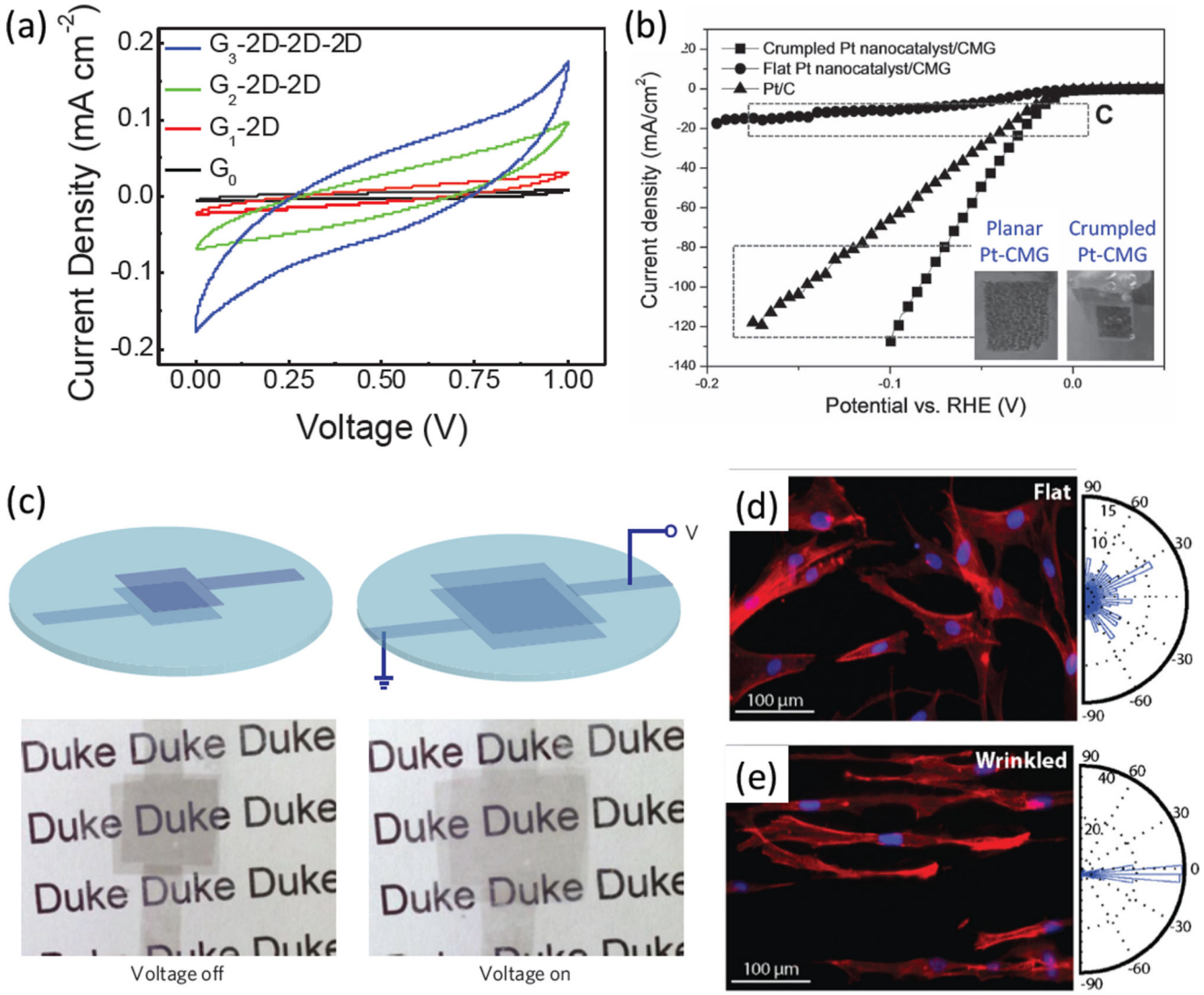

Figure 4. Technological advantages of wrinkled/crumpled graphene in various applications

(a) Electrochemical cells: CV curves of multigenerational graphene structures fabricated by sequential deformation. Hierarchical G_3 structure demonstrates a 20-time higher current density than planar G_0 film.[60] Reproduced with permission from ref. 60. Copyright 2016, Wiley-VCH. (b) Catalytic electrodes: HER of Pt nanocatalyst/crumpled chemical modified graphene (CMG) (squares), Pt nanocatalyst/flat graphene (circles), and Pt/C (triangles). The right inset images demonstrate the ease of H_2 release from crumpled Pt-graphene electrode.[64] Reproduced with permission from ref. 63. (c) Actuator: voltage-induced actuation of a crumpled graphene–elastomer composite. As a voltage is applied (right), the composite reduces its thickness and expands its area. The area actuation strain is over 100%.[46] Reproduced with permission from ref. 46. Copyright 2013, Nature Publishing Group. (d)(e) Biological functional surfaces: human fibroblast culture on flat and wrinkled graphene materials results in randomly shaped and highly aligned cells, respectively.[48] Reproduced with permission from ref. 48. Copyright 2016, Elsevier.

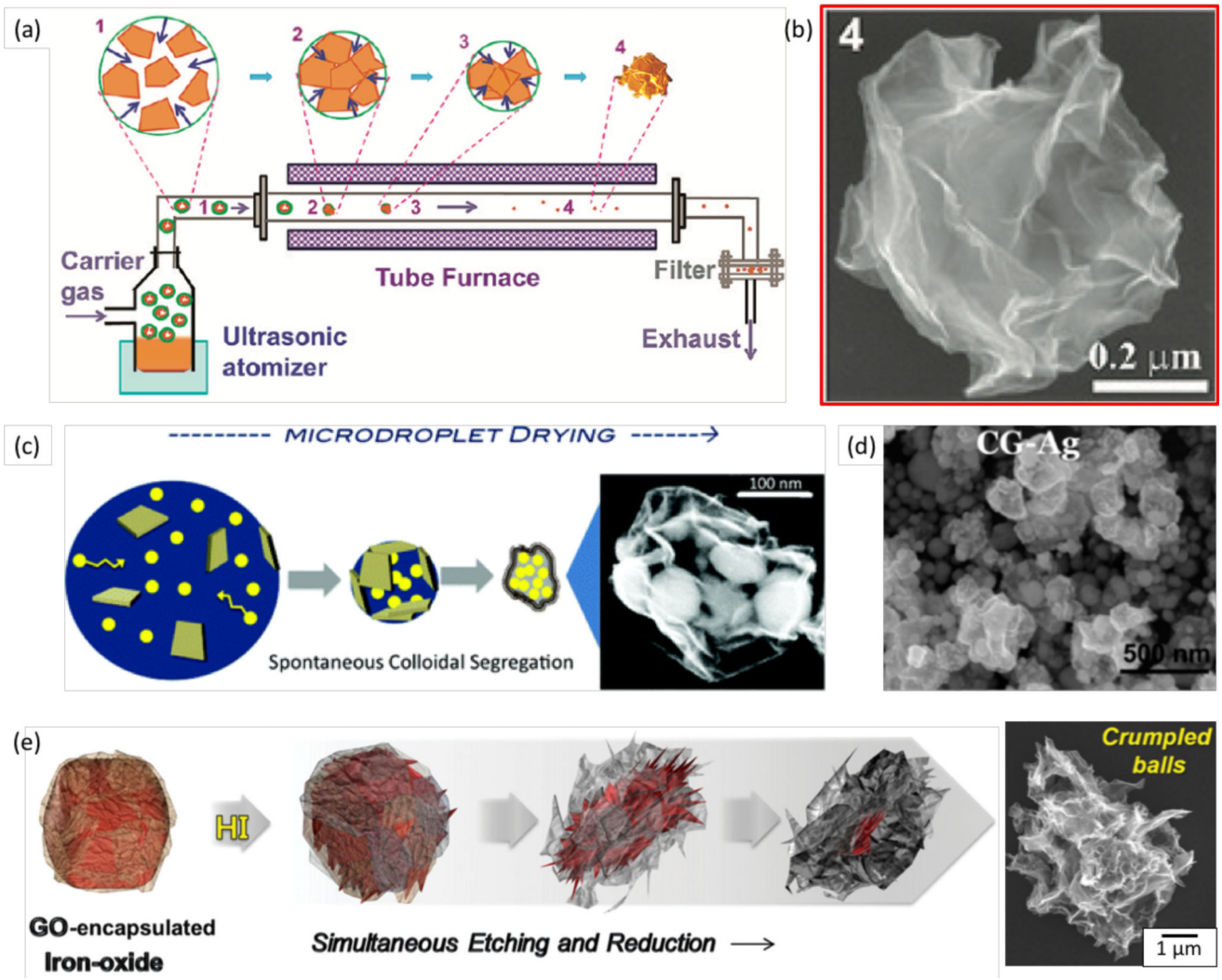

Figure 5. Crumpled nanosacks fabricated via capillary drying

(a) Schematic illustration represents an evaporation-induced process for the creation of crumpled nanosacks.[78] (b) SEM images of the final 3D crumpled, ball-like graphene nanosacks.[78] Reproduced with permission from ref. 78. Copyright 2011, American Chemical Society. (c) Schematic illustration of the assembly of cargo-filled graphene nanosacks by mixing the nanoparticles with GO dispersion prior to microdroplet drying. The inset SEM image shows Ag nanoparticles are wrapped with graphene sheets.[85] Reproduced with permission from ref. 85. Copyright 2012, American Chemical Society. (d) The SEM image of crumpled graphene-Ag nanocrystal nanosacks fabricated by mixing the GO dispersion with $AgNO_3$. The crumpling of GO sheets and nucleation of Ag nanoparticles occur in parallel.[86] Reproduced with permission from ref. 86. Copyright 2012, American Chemical Society. (e) Scheme of the templated synthesis that starts with the coating of GO sheets on iron oxide nanoparticles followed by HI etching. The inset SEM image shows the final crumpled graphene balls.[88] Reproduced with permission from ref. 88. Copyright 2016, Wiley-VCH.

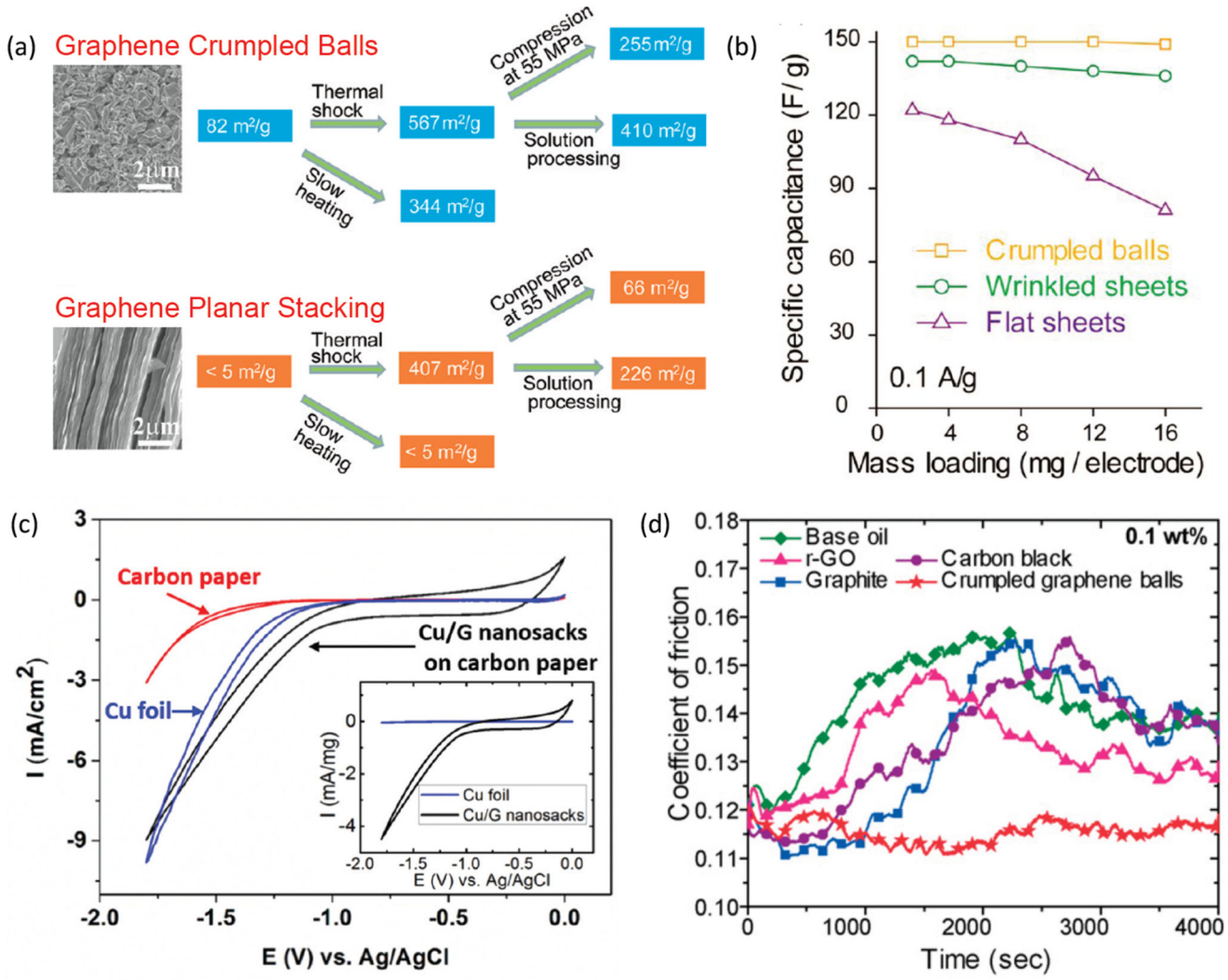

Figure 6. Superior performance of crumpled graphene microparticles in various technological applications

(a) Evolution of the specific surface areas of graphene crumpled balls and graphene planar stacking after various processing conditions including heating, solution processing, and mechanical compression.[78] Reproduced with permission from ref. 78. Copyright 2011, American Chemical Society. (b) Supercapacitor: specific capacitance (F g^{-1}) of the three graphene samples as a function of mass loading at current density of 0.1 A g^{-1}.[92] Reproduced with permission from ref. 92. Copyright 2013, American Chemical Society. (c) Catalytic reduction of CO_2: catalytic activity of Cu-graphene microparticles for the electrochemical reduction of CO_2 in 0.1 M aqueous $KHCO_3$. The inset plot shows the activity of the Cu foil and Cu-graphene hybrids normalized by copper mass, showing the much higher activity of the nanosack system.[87] Reproduced with permission from ref. 87. Copyright 2015, Royal Society of Chemistry. (d) Wear reduction: variation of coefficient of friction as a function of time using PAO4 base oil and with 0.1 wt. % crumpled graphene balls.[97] Reproduced with permission from ref. 97. Copyright 2016, National Academy of Sciences.

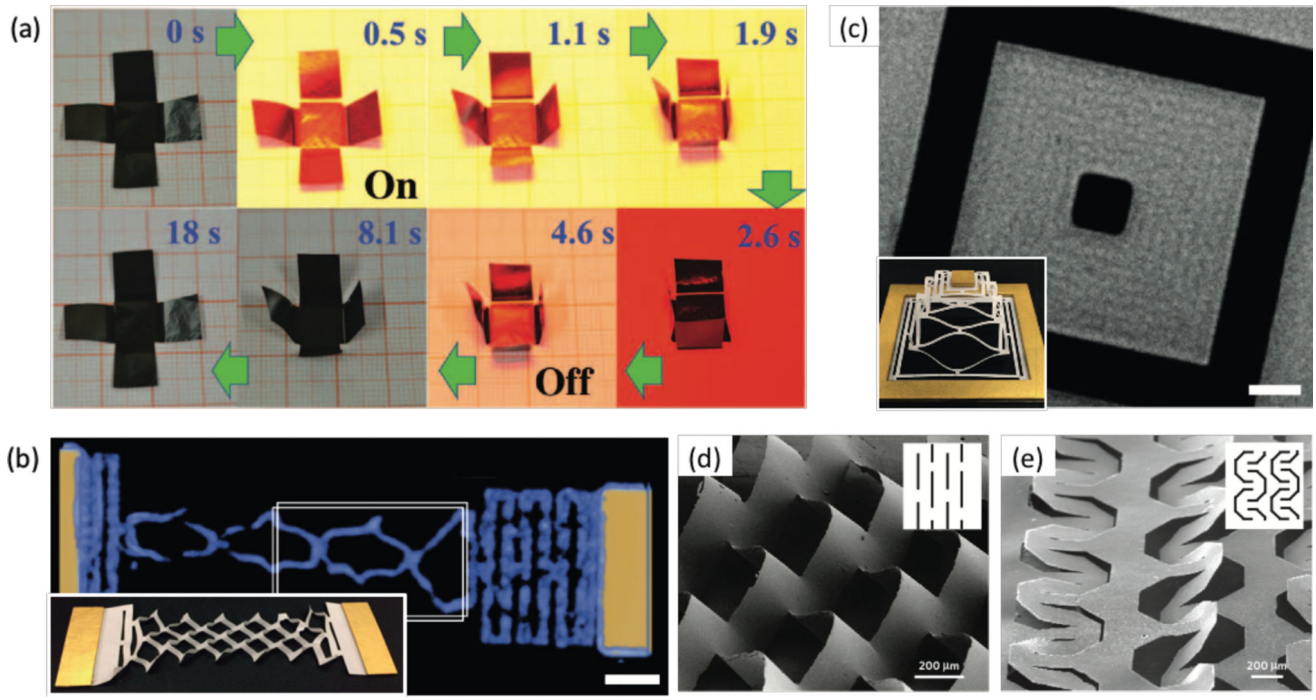

Figure 7. Graphene origami and kirigami structures

(a) A self-folding graphene origami box driven by light. Time profiles of self-folding movements of a graphene paper with and without NIR light irradiation.[103] Reproduced with permission from ref. 103. Copyright 2015, American Association for the Advancement of Science. (b) Graphene in-plane kirigami spring. Paper model of in-plane kirigami is shown in the inset. This graphene in-plane kirigami spring is actuated by external mechanical force. The scale bar for graphene kirigami is 10 μm.[105] (c) Paper model and as-fabricated graphene kirigami pyramid. The scale bar for graphene pyramid kirigami is 10 μm. This graphene out-of-plane spring is actuated by using an infrared laser.[105] Reproduced with permission from ref. 105. Copyright 2015, Nature Publishing Group. (d)(e) SEM images of two examples of microscale kirigami patterns in GO-PVA nanocomposites after photolithography. The insets show the corresponding kirigami unit cells.[106] Reproduced with permission from ref. 106. Copyright 2015, Nature Publishing Group.

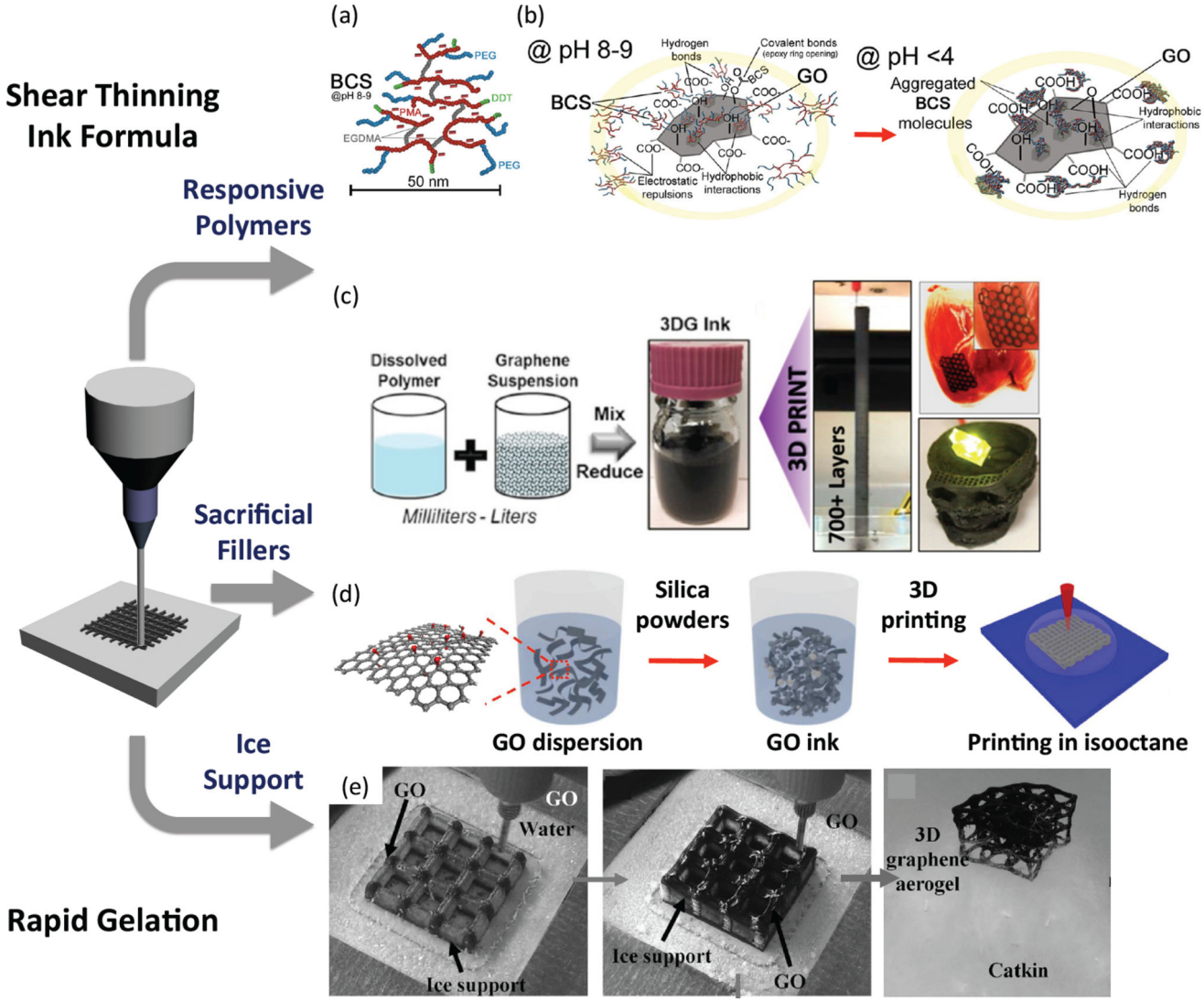

Figure 8. Printing in three dimensions

3D printing of 2D materials (*e.g.*, GO) requires precise control of rheology of GO-based inks. (a) Scheme of GO sheet and branched copolymer surfactant (BCS) in 3D printable ink.[115] (b) The GO-based ink is pH responsive: when the pH<4, the protonation of carboxyl groups of BCS leads to the formation of hydrogen bonds with GO sheets, directing the assembly of GO sheets into a 3D network.[115] Reproduced with permission from ref. 115. (c) Scheme of the preparation of silica-filled GO ink and 3D printing process.[116] Reproduced with permission from ref. 116. Copyright 2015, Nature Publishing Group. (d) Schematic illustration of a 3D printing technique using composite ink consisting of GO sheets and polylactide-co-glycolide. The resulting graphene structure is mechanically robust and electrically conductive.[117] Reproduced with permission from ref. 117. Copyright 2015, American Chemical Society. (e) Photo of rapid printing 3D graphene structures by freeze casting GO suspensions. The freeze cast GO turns into ultralight graphene aerogels after thermal reduction.[118] Reproduced with permission from ref. 118. Copyright 2016, Wiley-VCH.

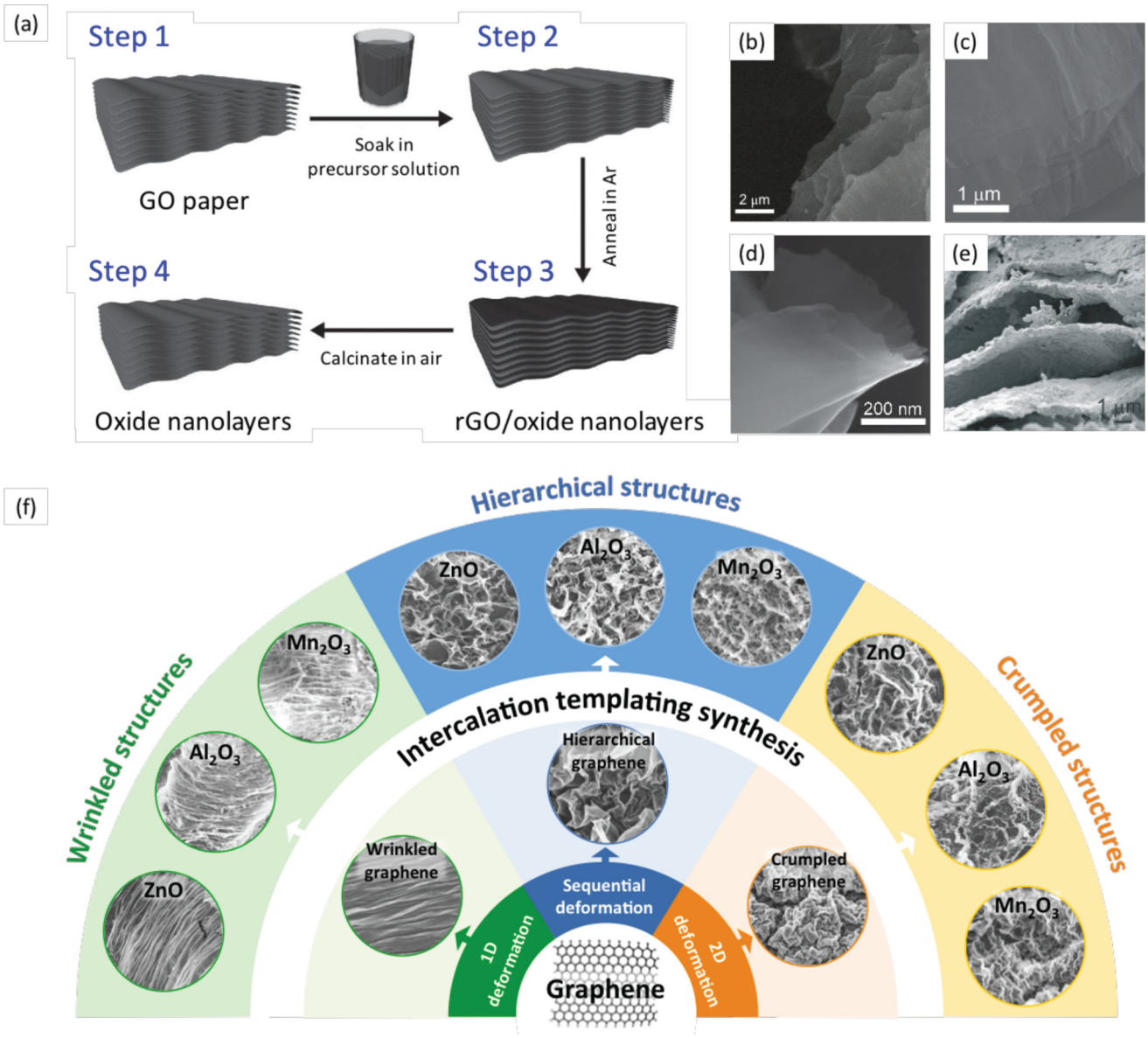

Figure 9. Intercalation templating synthesis for the creation of 2D metal oxides with higher dimensions

(a) Schematic illustration of the synthetic routes toward 2D metal oxide nanolayers.[143] As-templated (b) ZnO,[142] (c) Fe_2O_3[143] (d) TiO_2,[143] and (e) $YBa_2Cu_3O_{7-\delta}$ (Y123) layered structures.[144] Reproduced with permission from ref. 143. Reproduced with permission from ref. 142. Copyright 2015, Nature Publishing Group. Reproduced with permission from ref. 144. Copyright 2015, Royal Society of Chemistry. (f) Generalized synthetic routes for fabricating crumple/wrinkle-textured metal oxides. Pre-textured (wrinkled, crumpled, hierarchical) GO structures can be utilized as intercalation templates. After removing graphene-based templates, multiple textured metal oxides (ZnO, Al_2O_3, Mn_2O_3) are achieved with replicated wrinkled, crumpled, hierarchical structures. The radius of each

SEM is 20 μm.[145] Reproduced with permission from ref. 145. Copyright 2016, American Chemical Society.